



Universitat Politècnica de Catalunya  
Department of Civil and Environmental Engineering

# **CROSS SECTIONAL BEHAVIOR OF HOT-ROLLED I-SECTIONS OF AUSTENITIC STAINLESS STEEL SUBJECTED TO BIAXIAL LOADING**

***Supervised by:***  
Rolando Chacón Flores

***Student***  
Rosangela Fonseca Campagnuolo

Barcelona, May, 2017

*To Hernán and Filomena.*

# TABLE OF CONTENTS

<b>TABLE OF CONTENTS</b>	<b>iii</b>
<b>LIST OF FIGURES</b>	<b>v</b>
<b>LIST OF TABLES</b>	<b>vii</b>
<b>ACKNOWLEDGEMENTS</b>	<b>ix</b>
<b>Chapter 1</b>	<b>10</b>
<b>1.1. Background</b>	<b>11</b>
<b>1.2. Structural applications</b>	<b>12</b>
<b>1.3. Research Objectives</b>	<b>14</b>
1.3.1. General Objectives	14
1.3.2. Specific Objectives	15
<b>Chapter 2</b>	<b>16</b>
<b>2.1. Stainless Steel</b>	<b>16</b>
2.1.1. Types of Stainless Steel	16
2.1.2. Material Response	18
<b>2.2. Design Formulae</b>	<b>20</b>
2.2.1. Cross sectional assumptions by EN-1993-1-4 (2006).	21
<b>2.3. The Continuous Strength Method (CSM)</b>	<b>26</b>
<b>2.4. Previous experimental programs</b>	<b>28</b>
<b>Chapter 3</b>	<b>31</b>
<b>3.1. Experimental Data</b>	<b>31</b>
<b>3.2. Constitutive material equation</b>	<b>34</b>

3.3.	Basic modelling assumptions	37
3.4.	Model validation	38
3.5.	Conclusion remarks	39
<b>Chapter 4</b>		<b>41</b>
4.1.	Parametric study on Load application point.	41
4.2.	Parametric study on alpha and beta powers.	48
<b>Chapter 5</b>		<b>51</b>
5.1.	Phenomenological Insight	52
5.2.	Analysis of members subjected compression loading	55
5.3.	Analysis of members subjected eccentric loading	59
5.3.1.	Influence of variation of load application point	59
5.3.2.	Alpha and beta Analysis	66
5.4.1.	Sensitivity analysis to alpha and beta	68
<b>Chapter 6</b>		<b>71</b>
6.1.	Analysis of members subjected to compression loading.	72
6.2.	Analysis of members subjected to eccentric loading.	72
6.3.	Influence of load application point.	73
6.4.	Alpha and beta sensitivity analysis.	73
6.5.	Future research work	73
<b>Chapter 7</b>		<b>75</b>

## LIST OF FIGURES

<i>Figure 1. Girder bridge in Stockholm, Sweden.....</i>	<i>13</i>
<i>Figure 2. Arch bridge in York, England. ....</i>	<i>13</i>
<i>Figure 3. Through bridge in Bilbao, Spain.....</i>	<i>14</i>
<i>Figure 4. Composition of stainless steels alloys (British Stainless Steel Association).....</i>	<i>17</i>
<i>Figure 5. Buckling curves for flexural, torsional and flexural-torsional buckling. ....</i>	<i>25</i>
<i>Figure 6. Stub column load-deformation response by Liew, A. and Gardner, L. (2015).....</i>	<i>27</i>
<i>Figure 7. Schematic stress-strain curves for cold-formed material and the CSM material model. ....</i>	<i>27</i>
<i>Figure 8. Stub column test setup and position of the strain gauges. Zheng B (2015).....</i>	<i>33</i>
<i>Figure 9. Engineering and true Stress-Strain curves according to EN-1993-1-4. .</i>	<i>35</i>
<i>Figure 10. Engineering and true Stress-Strain curves according to Experiment. .</i>	<i>36</i>
<i>Figure 11. Ultimate Stresses according to EN-1993-1-4 and Experiment formulae. ....</i>	<i>36</i>
<i>Figure 12. Coupling constraint at +RP1 and +RP2 .....</i>	<i>38</i>
<i>Figure 13. Parametric study variables and combinatorics. ....</i>	<i>42</i>
<i>Figure 14. Modelling assumptions. ....</i>	<i>43</i>
<i>Figure 15. Python simplified subroutine. ....</i>	<i>44</i>
<i>Figure 16. Load-Displacements curve of a representative case <math>e=20\text{mm}</math>, <math>\vartheta=5^\circ</math>. .</i>	<i>47</i>

<i>Figure 17. Excel worksheet used to compute Parametric Study on alfa and beta.</i>	49
<i>Figure 18. Von Mises stresses due to compression loading L=500-350-250-200.</i>	52
<i>Figure 19. Structural response due to loading point ranging. L=250mm</i>	53
<i>Figure 20. Structural response due to loading point ranging. L=350mm</i>	54
<i>Figure 21. Local Buckling L=100 and L=200 mm.</i>	57
<i>Figure 22. Theoretical and numerical results reduction factor X.</i>	58
<i>Figure 23. Cross sectional behavior subjected to eccentric loading around from 0 to 360 degrees.</i>	59
<i>Figure 24. Influence of magnitude and angle variation, L=100mm.</i>	60
<i>Figure 25. Influence of magnitude and angle variation, L=200mm.</i>	60
<i>Figure 26. Influence of magnitude and angle variation, L=250mm.</i>	61
<i>Figure 27. Influence of magnitude and angle variation, L=350mm.</i>	62
<i>Figure 28. Influence of magnitude and angle variation, L=500mm.</i>	63
<i>Figure 29. Axial-Moment interaction.</i>	64
<i>Figure 30. Theoretical and numerical results.</i>	65
<i>Figure 31. Reduction of NEd,max due to alfa and beta exponents.</i>	67
<i>Figure 32. Sensitivity analisys case I</i>	68
<i>Figure 33. Sensitivity analisys case II</i>	69
<i>Figure 34. Influence of coefficient beta</i>	70

## LIST OF TABLES

<i>Table 1. Maximum width-to-thickness ratios for compression parts (internal compression parts) .....</i>	<i>21</i>
<i>Table 2. Maximum width-to-thickness ratios for compression parts (outstand flanges). .....</i>	<i>21</i>
<i>Table 3. Values of imperfection factor and non-dimensional slenderness for flexural buckling. ....</i>	<i>25</i>
<i>Table 4. CSM design powers <math>a_y</math>, <math>a_z</math>, <math>b_y</math>, <math>b_z</math>, <math>\alpha</math> and <math>\beta</math> for combined loading. Liew, A. and Gardner, L. (2015).....</i>	<i>28</i>
<i>Table 5. Test conducted on stainless steel beam columns .....</i>	<i>29</i>
<i>Table 6. Test conducted on stainless steel RHS and SHS members subjected to compression and combined loading.....</i>	<i>30</i>
<i>Table 7. Material properties obtained from coupon tensile test.....</i>	<i>32</i>
<i>Table 8. Test results beam column specimens.....</i>	<i>33</i>
<i>Table 9. Measured dimensions and imperfections for welded H specimens. ....</i>	<i>34</i>
<i>Table 10. Case I: EN-1993-1-4 formulae.....</i>	<i>34</i>
<i>Table 11. Case II: Experiment formulae.....</i>	<i>34</i>
<i>Table 12. Material properties sensitivity by ABAQUS. ....</i>	<i>36</i>
<i>Table 13. Test and Abaqus results of 80H specimens .....</i>	<i>39</i>
<i>Table 14. Non slenderness values related to length. ....</i>	<i>41</i>
<i>Table 15. Load-Displacements values of a representative single case <math>e=20\text{mm}</math>, <math>\vartheta=5^\circ</math>.....</i>	<i>45</i>
<i>Table 16. Numerical results from Abaqus .....</i>	<i>48</i>
<i>Table 17. Cases of study generated by Alfa and beta variations. ....</i>	<i>50</i>
<i>Table 18. Alfa and beta influence.....</i>	<i>50</i>

<i>Table 19. Maximun Von Mises stresses for L=250mm .....</i>	<i>53</i>
<i>Table 20. Maximun Von Mises stresses for L=350mm .....</i>	<i>54</i>
<i>Table 21. Non-dimensional slenderness and elastic critical force.....</i>	<i>56</i>
<i>Table 22. Theoretical and numerical values of reduction factor X.....</i>	<i>56</i>
<i>Table 23. Influence of <math>\sigma_{0.2\%}</math> according to EN-1993-1-4 and Abaqus.....</i>	<i>58</i>
<i>Table 24. Theoretical and numerical response .....</i>	<i>65</i>
<i>Table 25. Reduction of <math>N_{Ed,max}</math> due to alfa and beta exponents.....</i>	<i>66</i>
<i>Table 26. Verification of Strain ratio of members .....</i>	<i>68</i>



## ACKNOWLEDGEMENTS

To my parents for being my blessing and inspiration, for always reminding me that life is about overcoming, that patience, hard-working, optimism and commitment are the keys of success.

To my family, for the endless manifestations of love, esteem and motivation expressed since I decided to leave Venezuela. For reminding me that distance makes each get-together priceless.

To all my friends, those who started this adventure with me, those who remain despite the distance and those who are no longer, thank you all for being part of this great challenge and fulfill me with positive energy and encouraging words.

To my supervisor Rolando Chacón for the continued support, guidance and encouragement. For pursuing excellence and quality in every step of this study.

To *GPO Ingeniería i Arquitectura* for being my first professional experience abroad and for allowing me to assist to my weekly- tutorials. This opportunity was a great chance for learning and professional development.

**Chapter 1**  
**INTRODUCTION**

## 1.1. Background

Over the past two decades, application of stainless steel in civil engineering structures has increased significantly. Far across the high initial cost that implied its use as a structural material- approximately four times that of carbon steel- stainless steel is characterized by its excellent performance in terms of corrosion and fire resistance, maintenance, superior durability, aesthetics and low cost life-cycle.

Variation of chemical composition and heat treatments allow the metallurgic industry to produce different grades of stainless steel. According to their metallurgical structure, stainless steel is classified in five mains groups namely: austenitic, ferritic, duplex (austenitic ferritic), martensitic, and precipitation hardening.

Austenitic stainless steel is one of the most common and high cost grades used for construction-applications, is manly made of chromium and nickel, the responsible for the corrosion resistance property and its reasonable high cost. Unfortunately the pricing of stainless steel will be affected by the worldwide price of nickel, while nickel demand remained strong austenitic stainless steel will still being a commodity with high market fluctuations.

On the other hand, austenitic stainless steel exhibits greater thermal expansion and heat capacity, with lower thermal conductivity than other stainless or conventional steels. They are generally readily welded, but care is required in the selection of consumables and practices for more highly alloyed grades

Stainless steel differs from carbon steel in its non-linear stress-strain property, therefore structural design codes for carbon steel should not be applied directly to stainless steel due to the lack of special strength and stiffness properties.

Nevertheless, it is common to assume that the behavior of stainless steels grades is similar to that exhibited by carbon steel design rules. Studies of structural cross-sections often include simplifications, allowing fast and conservative estimates of capacity to be calculated. The objective of this

study is to assess the design approach codes used to evaluate cross-sectional behavior of I welded elements under biaxial bending in order to achieve a better understanding of the interaction formulae given in EN-1993-1-3 (2006).

## **1.2. Structural applications**

Historically, the aesthetics of stainless steel has been an important factor in its specification for structural and architectural applications. Consequently, many existing examples of stainless steel structures display a high level of exposed structural members, commonly of tubular cross-section, and are often of a prestigious or landmark nature.

For structural members, the most commonly used products are cold-formed section, due to their low investment to achieve production capabilities, readily availability and suitability for light structural applications with high structural and material efficiency. Therefore hot-rolled and build-up sections are relatively scarce, though structural design guidance is available.

As mentioned above, stainless steel is generally welded but requires careful selection of consumables and practices for more highly alloyed grades. In order to highlight stainless steel properties, some cross-section which are made from individual hot-rolled plates of stainless steel welded together used in structural applications are shown according to Euro Inox (2004).

### *Girder bridge in Stockholm, Sweden.*

Located over the Sickla Canal in the south of Stockholm, the bridge frame is made of high-strength duplex steel (grade:1.4462) due to the high salt content in the water flowing in from the Baltic, with a box girder of triangular cross-section which is made from individual hot-rolled plates of stainless steel welded together.

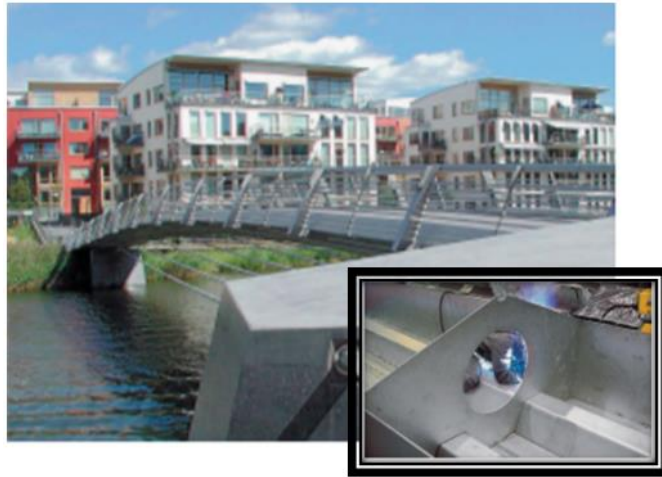


Figure 1. Girder bridge in Stockholm, Sweden.

Arch bridge in York, England.

This bridge over the River Ouse at York has a stainless steel arch with a slender bridge deck suspended from a radial arrangement of stainless steel cables, with a polygonal cross section deck which is made of welded stainless steel plates.



Figure 2. Arch bridge in York, England.

Through bridge in Bilbao, Spain.

This footbridge spans River Nervión, linking Deusto University with the district of Abandoibarra has a support structure made of duplex stainless steel, grade 1.4362. The U-shaped trough is made up of stainless steel plate, with welded

reinforcing ribs on the underside. Welded box beam on the upper and lower edges brace the bridge in a longitudinal direction.



Figure 3. Through bridge in Bilbao, Spain.

### 1.3. Research Objectives

The purpose of this study is to understand the cross sectional capacity of stainless steel I-Welded sections subjected to eccentric load and to provide efficient recommendations to the current design specifications. General and specific objectives are described in this section.

#### 1.3.1. General Objectives

The stress-strain behavior of structural steel can differ depending on the material grade, the manufacturing processes involved in its fabrication. These might involve mechanical procedures and different testing methods hot rolling or cold forming, affecting the material's behavior by alternating the distinctiveness of yield point. Variations in material properties and behavior around structural cross-sections are also possible.

The design methods used to compute cross-sectional capacity given by EN-1993-1-1 (2005) and the American code AISI. (2012) are the same of the corresponding low carbon steel design specification. Mirroring behavior of stainless steel to carbon steel can produce potential disadvantage of being overly conservative increasing design costs and avoid efficient designs.

Similarly, several experimental and numerical tests have been conducted to structural steel cold-formed members under pure axial compression, pure bending and combined loading. Nevertheless, biaxial bending differs from the basic case of axial load or uniaxial bending behavior and there are not many studies showing the ultimate resistance of stainless steel welded I cross section. In order to verify accuracy and reduce scatter of EN-1993-1-4 (2006) design strength, this study has as the main objective of understanding the ultimate capacity of stainless steel I- welded cross-section under biaxial bending using the nonlinear interaction formula given by EN-1993-1-1 (2005) for I sections.

### 1.3.2. Specific Objectives

The specific objectives of this study are the following:

- To identify the accuracy of the current design specification EN-1993-1-4 (2006) related to stainless steel material response, comparing theoretical results obtained by the use of equation C-1 of Annex C of EN-1993-1-4 (2006) with experimental data.
- To strengthen the use of numerical tools based upon complex Finite Element, 3D Models and continuum mechanics in the particular field of steel structures.
- To compare the ultimate load capacity of cross sections members subjected to pure compression and biaxial loading given by EN-1993-1-1 (2005) with ultimate load obtained of numerical modelling, giving ratios between theoretical and numerical results , in order to define the most accurate and efficient design approach for stainless steel I welded sections.
- To validate accuracy of alfa and beta exponential values for I and H stainless steel cross section under biaxial bending proposed by EN-1993-1-1 (2005) by means of numerical analysis.
- To identify future line research related to the cross-sectional stainless steel welded profiles.

## Chapter 2

### STATE OF ART

#### 2.1. Stainless Steel

This chapter presents a sort report of the literature review related to this study.

A brief description of Stainless steel, types, grades and properties is first presented, followed by their material response and stress-strain behavior. Then, design formulae proposed by European Standard, stainless steel cross section behavior and formulae used to assess members subjected to compression and biaxial loading. Continuing with a description of the Continuous strength method is also shown. Finally a summary of the most representative previous experimental programs of stainless steel is covered.

##### 2.1.1. Types of Stainless Steel

According to their metallurgical structure, stainless steel is classified in five main groups namely: austenitic, ferritic, duplex (austenitic ferritic), martensitic, and precipitation hardening. A lot of high-alloy steels are designed with the help of the Schaeffler diagram (*Figure 4*). It shows composition of stainless steels according to alloying elements equivalent-content Nickel and Chromium.



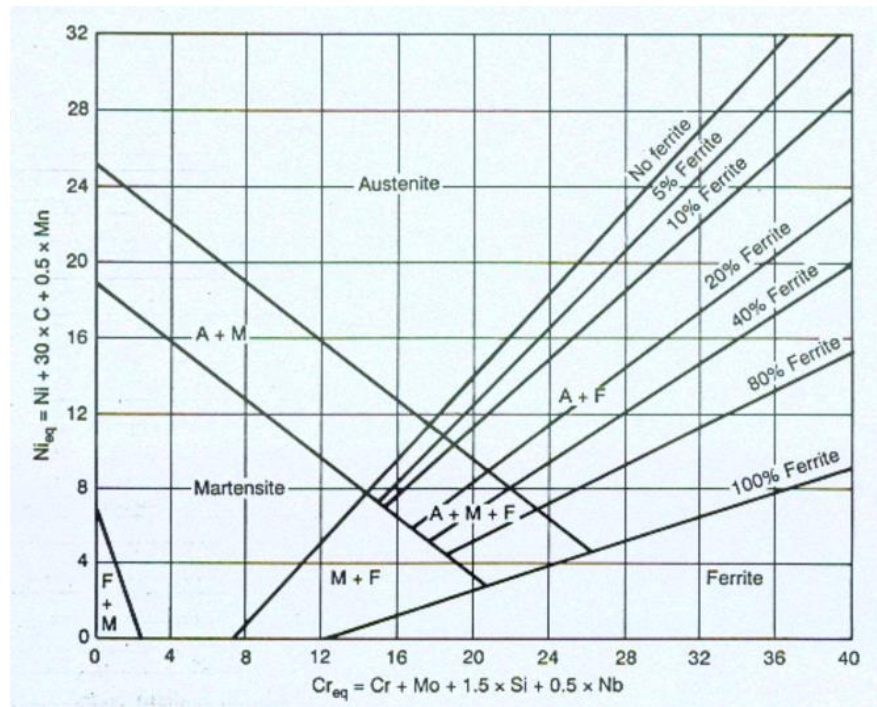


Figure 4. Composition of stainless steel alloys (British Stainless Steel Association)

Ferritic steels are defined by a body-centered cubic (BCC) grain structure, which means that the crystal structure of such steels is comprised of a cubic atom cell with an atom in the center. This grain structure is responsible of ferritic steels magnetic properties. It is important to know magnetism in metals is created by the uneven distribution of electrons in atoms of certain metal elements. When magnetic dipoles align they create a magnetic domain, a localized magnetic area that has a north and a south pole.

Although ferritic steels cannot be hardened or strengthened by heat treatment, have good resistance to stress-corrosion cracking. They can be cold worked and softened by annealing and rich a high yield stress also called 0.2% proof stress of 250-330 MPa in the annealed condition. While not as strong or corrosion resistant as austenitic grades, the ferritic grades generally have better engineering properties and due to their lower chromium and nickel content, standard ferritic steel grades are usually less expensive than austenitic. Though generally very weldable, some ferritic steel grades can be prone to sensitization of the weld heat-affected zone and weld metal hot cracking. Weldability limitations, therefore, restrict the use of these steels to thinner gauges.

In comparison with ferritic stainless steel, and according to ASM International (2008), Austenitic stainless steels are the most common and familiar types of stainless steel characterized by the formable and weldable properties, simply recognized as nonmagnetic: unmagnetized materials, magnetic domains face in different directions, canceling each other out.

Austenitic stainless steel can be positively used from cryogenic temperatures to the red-hot temperatures of heaters and jet engines. The amount of chromium contained is about 16 and 25%, and they also contain nitrogen in solution, both of which contribute to their high corrosion resistance. Were it not for the cost of the nickel that helps stabilize their austenitic structure, these alloys would be used even more widely.

From a metallurgical point of view, the use of Austenitic stainless steels have advantages in terms of strength because they can be made soft enough, with yield stress also called 0.2% proof stress of about 200 MPa, to be easily formed by the same tools that work with carbon steel, but they can also be made incredibly strong by cold work, up to yield strengths of over 2000 MPa. Their austenitic (fcc, face-centered cubic) structure is very tough and ductile down to absolute zero. They also do not lose their strength at high temperatures as fast as ferritic. The least corrosion-resistant versions can endure the normal corrosive attack of the everyday environment, while the most corrosion-resistant grades can even withstand boiling seawater.

### 2.1.2. Material Response

Stainless steels exhibit a linear elastic behavior up to the yield stress and a pronounced yield plateau before strain hardening is found, while stainless steel is characterized by a rounded stress-strain response with no sharply defined yield point. For that, to mirror material response an equivalent yield stress is used in structural design, commonly chosen as a suitable proof stress. Stainless steel yield point strengths is named as  $\sigma_{0.2}$  which is defined for an offset permanent strain conservatively the 0.2% strain.

Stainless steel behavior has represented analytically by different material models, which have been sophisticated over time to find accurate response.

The most popular description of the stress-strain response on non-linear material is based on the well-known Ramberg-Osgood (1941) formula. This formulae describes the full range strain hardening behavior of steels. The stress-strain curve is defining using Eq [1]. However, Ramberg-Osgood expression generally provides close approximations to measured stress-strain curves for stresses up to the 0.2% proof stress, but was find that expression become really inaccurate due to they are extrapolations of curve fits to stresses lower than the 0.2% proof stress.

$$\varepsilon = \frac{\sigma}{E_0} + 0.002 \left( \frac{\sigma}{\sigma_{0.2}} \right)^n \quad \sigma \leq \sigma_{0.2} \quad [1]$$

In order to improve accuracy, Mirambell and Real (2000) proposed a material mode, which was later modified by Rasmussen (2003) and included in Annex C of EN1993-1-4 (2006) defining a second curve for stresses above the 0.2% proof stress given by Eq. [2], [3], with an additional strain hardening exponent  $m$  for the second stage.

$$\varepsilon = \frac{\sigma}{E_0} + 0.002 \left( \frac{\sigma}{f_y} \right)^n \quad \sigma \leq f_y \quad [2]$$

$$\varepsilon = 0.002 + \frac{f_y}{E} + \frac{\sigma - f_y}{E_y} + \varepsilon_u \left( \frac{\sigma - f_y}{f_u - f_y} \right)^m \quad f_y \leq \sigma \leq f_u \quad [3]$$

Where  $n$  is a coefficient defined as [4],  $R_{0.01}$  is the 0.01% proof stress,  $n$  may be taken from table Table 4.1 of EN1993-1-4 (2006) or may be calculated from measured properties.  $E_y$  is the tangent modulus of the stress-Strain curve at the yield strength leading Eq. [5].  $\varepsilon_u$  is the ultimate strain, corresponding to the ultimate strength  $f_u$ , where  $\varepsilon_u$  may be obtained from the approximation of [6] and  $m$  is also a coefficient defined as [7]

$$n = \frac{\ln(20)}{\ln\left(\frac{f_y}{R_{0.01}}\right)} \quad [4]$$

$$E_y = \frac{E}{1 + 0.002n \frac{E}{f_y}} \quad [5]$$

$$\varepsilon_u = 1 - \frac{f_y}{f_u} \quad [6]$$

$$m = 1 + 1.35 \frac{f_y}{f_u} \quad [7]$$

Finally, Gardner and Ashraf (2006) modified the two-stage material model adopted by Annex C of EN1993-1-4 (2006) with the purpose of increasing the accuracy of the model at low strains, approximately less than 10% and to allow the use of this curve to compressive stress-strain behavior. The variations presented by the researchers involved the use of the 1% proof stress instead of the ultimate stress in the second stage of the model as shows Eq. [8] In this equation  $\sigma$  and  $\varepsilon$  are the engineering stress and strain respectively,  $E_o$  is the initial Young's modulus,  $\sigma_{0.2}$  is the 0.2% proof stress, also called yield stress,  $n$  is a strain hardening exponent,  $\sigma_{1.0}$  is the 1% proof stress and  $n_{0.2,1.0}$  is a strain hardening coefficient representing a curve that passes through  $\sigma_{0.2}$  and  $\sigma_{1.0}$ .

$$\varepsilon = \frac{\sigma - \sigma_{0.2}}{E_o} + \left(0.008 - \frac{\sigma_{0.1} - \sigma_{0.2}}{E_{0.2}}\right) \left(\frac{\sigma - \sigma_{0.2}}{\sigma_{0.1} - \sigma_{0.2}}\right)^{n_{0.2,0.1}} + \varepsilon_{t0,2} \quad \sigma_{0.2} \leq \sigma \leq \sigma_u \quad [8]$$

$$E_{0.2} = \frac{E}{1 + 0.002n \frac{E}{\sigma_{0.2}}} \quad [9]$$

## 2.2. Design Formulae

Structural applications of stainless steel are becoming increasingly frequent. Several specifications are available for the design of stainless beam-columns, including the American code AISI. (2012) and the Australian/New Zealand standard (AS/N25 4673-2001) for cold formed members and the Eurocode EN 1993-1-4 (2006) for cold formed and welded members.

This study focuses their attention to the guidance provided by European standard EN1993-1-4 (2006). It is well know that the most of the design methods described in this specification are the same as those in their corresponding low carbon steel design specifications EN1993-1-1 (2005) (e.g. The ultimate capacity of stainless steel sections through the cross-section classification for the treatment of local buckling, the ultimate capacity of cross section under pure compression, biaxial bending, etc.). Nevertheless the value of buckling curves which represent residual stresses and initial

imperfections factor and limiting slenderness differs from those recommended in carbon steel design specifications.

### 2.2.1. Cross sectional assumptions by EN-1993-1-4 (2006).

#### Cross Sectional classification

The European structural stainless steel design standard EN1993-1-4 (2006) classify sections based on their moment-rotation capacity and also specify the maximum or limiting width-to-thickness ratio  $c/t$ , which depends on the highest (least favorable) class of its constituent parts that are partially or wholly in compression: internal compression parts and outstand flanges.

Table 1 and Table 2 shows the limiting values width-to-thickness ratio  $c/t$  given by EN-1993-1-1 and EN-1993-1-4 respectively. Carbon Steel code gives more conservative limits than Stainless steel code.

Table 1. Maximum width-to-thickness ratios for compression parts (internal compression parts).

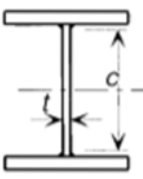
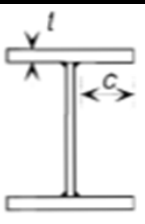
Internal compression parts					
	Class	EN-1993-1-1		EN-1993-1-4	
		Part subjected to bendig	Part subjected to compression	Part subjected to bendig	Part subjected to compression
	1	$c/t \leq 72\epsilon$	$c/t \leq 33\epsilon$	$c/t \leq 56\epsilon$	$c/t \leq 25.7\epsilon$
	2	$c/t \leq 83\epsilon$	$c/t \leq 38\epsilon$	$c/t \leq 58.2\epsilon$	$c/t \leq 26.7\epsilon$
	3	$c/t \leq 124\epsilon$	$c/t \leq 42\epsilon$	$c/t \leq 74.8\epsilon$	$c/t \leq 30.7\epsilon$

Table 2. Maximum width-to-thickness ratios for compression parts (outstand flanges).

Outstand Flanges			
	Class	EN-1993-1-1	EN-1993-1-4
		Part subjected to compression	Part subjected to compression
	1	$c/t \leq 9\epsilon$	$c/t \leq 9\epsilon$
	2	$c/t \leq 10\epsilon$	$c/t \leq 9.4\epsilon$
	3	$c/t \leq 14\epsilon$	$c/t \leq 11\epsilon$

Those compression elements that do not meet the criteria for Class 3 should be classified as Class 4 elements.

Below is shown a brief summary of the concepts given by EuroInox (2006) related to cross-sectional classifications:

**Class 1 cross-sections** are those which can form a plastic hinge with the rotation capacity required from plastic analysis.

**Class 2 cross-sections** are those which can develop their plastic moment resistance, but have limited rotation capacity.

**Class 3 cross-sections** are those in which the calculated stress in the extreme compression fiber of the steel member can reach its yield strength, but local buckling is liable to prevent development of the plastic moment resistance.

**Class 4 cross-sections** are those in which local buckling will occur before the attainment of yield stress in one or more parts of the cross-section.

### Cross sectional resistance

The design provision for carbon steel cross-sections under combined axial load and bending moment, are based on the first yield theory, as assumed in most international design standards, where failure is due to a linear interaction represented through a sum of the utilization ratios under each component of loading at any point in the cross-section reaching the limit value of unity. The theory is equally presented for the cross-sectional resistance of stainless steel.

The resistance of a cross-section subjected to compression,  $N_{c,Rd}$ , with a resulting force acting through the centroid of the gross section is given by EN-

1993-1-3 as  $N_{c,Rd} \leq \frac{Af_y}{\gamma_{M0}}$  (for Class 1, 2 and 3 cross-sections) and  $N_{c,Rd} \leq \frac{A_{eff}f_y}{\gamma_{M0}}$  assuming the effective section for Class 4 cross-sections.

For cross-sections subjected to a combination of loads, the European code EN1993-1-1 (2005) proposed the use of a more efficient I- and H- cross-section interaction formulae for Class 1 and 2 sections, derived by Rubin (1978) and Lindner (1984, 1997, 2003) by assuming full plasticity throughout the cross-section at failure.

The corresponding interaction formulae for I- and H- sections under major axis bending plus compression, minor axis bending plus compression and biaxial bending plus compression, are given by Equations [10]-[12]. where  $M_{pl,y,Rd}$  and  $M_{pl,z,Rd}$  the reduced plastic moment capacities about each principal axis due to the presence of the axial compressive load  $N_{Ed}$ ,  $n = \frac{N_{Ed}}{N_{pl,Rd}}$  is the ratio of the applied axial load to the cross-section yield load,  $a = \frac{(A - 2bt_f)}{A}$  is the ratio of the flange area to gross area of the cross-section considered  $a \leq 0.5$ ,  $\alpha$  and  $\beta$  are the interaction coefficients for biaxial bending which may conservatively be taken as unity or as  $\alpha = 2$ ;  $\beta = 5n$  but ;  $\beta \geq 1$

$$M_{N,y,Rd} = M_{pl,y,Rd} \left[ \frac{(1-n)}{(1-0.5a)} \right], \quad \text{but } M_{N,y,Rd} \leq M_{pl,y,Rd} \quad [10]$$

$$M_{N,z,Rd} = M_{pl,z,Rd} \left[ 1 - \left( \frac{n-a}{1-a} \right)^2 \right] \quad [11]$$

$$\left[ \frac{M_{y,Ed}}{M_{N,y,Rd}} \right]^\alpha + \left[ \frac{M_{z,Ed}}{M_{N,z,Rd}} \right]^\beta \leq 1 \quad [12]$$

### Strain hardening in cross sectional resistance

According to EuroInox (2006) work-hardening associated with cold forming operations during fabrication will generally increase the cross-sectional resistance but sufficient data are not yet available for stainless steel to enable design recommendations to be made. It is suggested that when the benefits of work-hardening are to be utilized, the cross-sectional resistance should be established by tests. EN1990 'Design Assisted by tested', Annex D also provides guidance for such design alternative.

In some situations, it is permissible to recognize the benefits of the strain hardening properties of stainless steel more fully in design. This may be achieved by utilizing an enhanced proof stress,  $\sigma_0$ , in place of the 0,2% proof stress  $f_y$  in all calculations. It is recommended that in the absence of a more detailed appraisal, perhaps involving non-linear finite element analysis, the following restrictions should be observed:

-The cross-section should be of Class 1 or Class 2 as calculated by using  $\sigma_0$  in place of  $f_y$  when calculating  $\varepsilon$  in *Tables 1-2*.

-The cross-section is subjected to major axis bending only.

-The member concerned is not subjected to instability caused by any form of buckling (flexural, torsional, lateral-torsional or distortional), again using  $\sigma_0$  in all calculations

### Member buckling resistance

In addition to the cross-sectional resistance, if some limiting values proposed EN-1993-1-4 (2006) are exceeded, consideration should be given to overall buckling of members, as addressed in this section. The resistance to flexural buckling should be determined from  $N_{b,Rd} = \frac{\chi A \sigma_{0.2}}{\gamma_{M1}}$  for Class 1, 2 and 3 cross-sections and  $N_{b,Rd} = \frac{\chi A_{eff} \sigma_{0.2}}{\gamma_{M1}}$  for Class 4 cross-sections. Where  $A$  is the gross area,  $A_{eff}$  is the effective area of Class cross-section and  $\chi$  is the reduction factor accounting for buckling, given by:

$$\chi = \frac{1}{\phi + [\phi^2 - \bar{\lambda}^2]^{0.5}} \leq 1 \quad [13]$$

$$\text{with } \phi = 0.5(1 + \alpha(\bar{\lambda} - \bar{\lambda}_o) + \bar{\lambda}^2) \quad [14]$$

$$\text{where } \bar{\lambda} = \sqrt{\frac{A \sigma_{0.2}}{N_{cr}}} \text{ for Class 1, 2 and 3 cross-sections [15]}$$

$$\bar{\lambda} = \sqrt{\frac{A_{eff} \sigma_{0.2}}{N_{cr}}} \text{ for Class 4 cross-sections [16]}$$

Where  $\alpha$  is the imperfection factor for flexural buckling mode on welded open sections acting on the minor axis  $\alpha=0.76$  and the limiting non-dimensional slenderness  $\bar{\lambda}_o = 0.20$ , both defined in *Table 3*.  $\sigma_{0.2}$  is the 0.2% proof stress and  $N_{cr}$  is the elastic critical force for the relevant buckling mode based on the gross cross sectional properties. The imperfection factor for flexural buckling mode is also show in *Figure 5*.



Buckling mode	Type of member	$\alpha$	$\bar{\lambda}_0$
Flexural	Cold formed open sections	0,49	0,40
	Hollow sections (welded and seamless)	0,49	0,40
	Welded open sections (major axis)	0,49	0,20
	Welded open sections (minor axis)	0,76	0,20
Torsional and torsional-flexural	All members	0,34	0,20

Table 3. Values of imperfection factor and non-dimensional slenderness for flexural buckling.

For non-dimensional slenderness  $\bar{\lambda} \leq \bar{\lambda}_0$  or for  $\frac{N_{Ed}}{N_{cr}} \leq \bar{\lambda}_0^2$  the buckling effects may be ignored and only cross sectional checks apply.

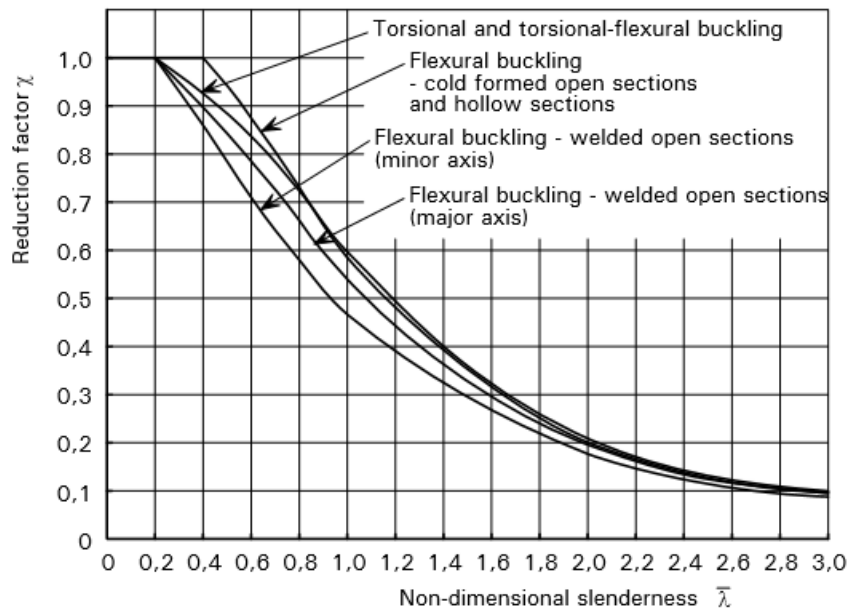


Figure 5. Buckling curves for flexural, torsional and flexural-torsional buckling.

To satisfy of cross-sectional resistance requirements at every point along member length and general requirements for beam members, interaction effects should be considered between compression loads and bending moments. According to EN-1993-1-4 for Axial compression and biaxial moments all members should satisfy equation [17]. Where  $e_{Ny}$  and  $e_{Nz}$  are the shifts in the neutral axes when the cross-section is subject to uniform compression.  $N_{Ed}$ ,  $M_{y,Ed}$  and  $M_{z,Ed}$  are the design values of the compression force and the maximum moments about the y-y and z-z axis along the member, respectively.  $(N_{b,Rd})_{min}$  is the smallest value of  $N_{b,Rd}$  for the following

three buckling modes: flexural buckling about the z axis, torsional buckling and torsional-flexural buckling.  $\beta_{W,y}$  and  $\beta_{W,z}$  are the values of  $\beta_W$  determined for the y and z axes respectively in which  $\beta_W = 1$  for Class 1 or 2 cross-sections.  $W_{pl,y}$  and  $W_{pl,z}$  are the plastic module for the y and z axes respectively.  $M_{b,Rd}$  is the lateral-torsional buckling resistance and  $k_y, k_z, k_{LT}$  are the interaction factors, where  $k_{LT}$  is equal to 1.0. This interaction formulae is shown on a theoretical effects, however its assessment on stainless steel members is not part of the study objectives.

$$\frac{N_{Ed}}{(N_{b,Rd})_{min}} + k_y \left( \frac{M_{y,Ed} + N_{Ed} e_{Ny}}{B_{w,y} W_{pl,y} f_y / \gamma_{M1}} \right) + k_z \left( \frac{M_{z,Ed} + N_{Ed} e_{Nz}}{B_{w,z} W_{pl,z} f_y / \gamma_{M1}} \right) \leq 1 \quad [17]$$

### 2.3. The Continuous Strength Method (CSM)

The continuous strength method (CSM), initially proposed by Gardner (2002) and Gardner and Nethercot (2004a), and further developed by Gardner and Ashraf (2006), Ashraf et al. (2006b, 2008a) and Gardner (2008b), further and continuous development by Afshan and Gardner (2013b), is a deformation-based design approach, allowing for strain hardening in the determination of cross-section compression and bending moment capacities. The CSM is a based design method with two key components: material model that allows for the influence of strain hardening and a base curve, which defines the maximum strain that a cross section can endure as a function of the cross-section slenderness. The method has been previously developed for predicting compression and bending resistance in isolation. Liew, A. and Gardner, L. (2015) extended CSM to the case of combined loading where analyses have been performed for structural steel I-sections a strain based numerical model and rationalized with simple equations suitable for use in design.

For the following study, some recommendations stated in Liew, A. and Gardner, L. (2015) must be taking into consideration to further result analysis.

For stub column load-deformation curves ( $N-\delta$ ), as shown in *Figure 6* Loads above the yield load will be reached if the cross-section slenderness is

sufficiently low to allow stresses to enter the strain hardening regime. The end shortening  $\delta$  at the ultimate load  $N_{lb}$  (i.e: the peak load  $N_{lb}$  achieved in the stub column test) is divided by the length of the specimen to obtain the average failure strain of the cross section  $\epsilon_{lb}$ . The deformation capacity of the stub column is defined as  $\epsilon_{CSM}$ , which is taken directly as  $\epsilon_{lb}$  for materials that exhibit a distinct yield point as  $\epsilon_{lb} - 0.002$  for materials with a rounded stress-strain curve. The subtraction of 0.2% strain in the case of rounded stress-strain curves is to ensure compatibility with the chosen material model *Figure 7* and to avoid over predictions of capacity

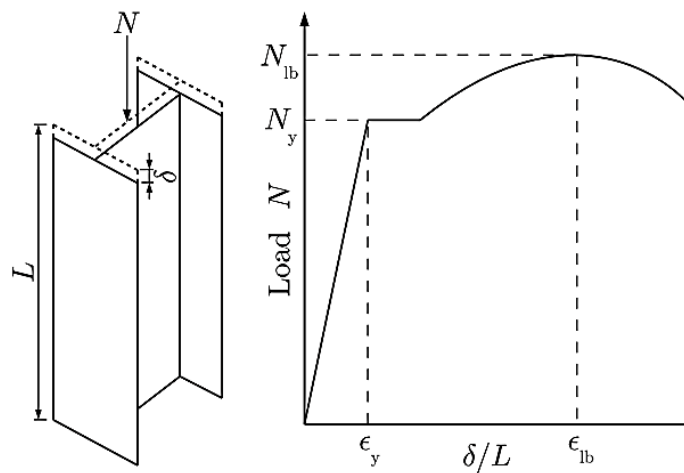


Figure 6. Stub column load-deformation response by Liew, A. and Gardner, L. (2015).

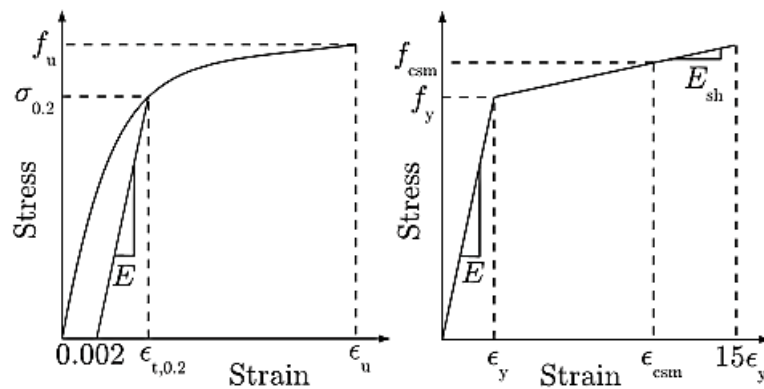


Figure 7. Schematic stress-strain curves for cold-formed material and the CSM material model.

Furthermore, the proposed form of design equations stated by Liew, A. and Gardner, L. (2015) given by Eqns. [17]-[19], trace bi-axial bending interaction curves that are anchored by reduced moments  $M_{R,CSM,y}$  and  $M_{R,CSM,z}$  which are functions of the axial load level  $n = \frac{N}{N_{CSM}}$ . Eqn. [18] contains two reduced

moment normalized in terms for major and minor axis bending raised to powers  $\alpha$  and  $\beta$  respectively. The equations are of a similar format to the design provisions in EN 1993-1-1-(2005) for combined axial load and bending moments. The equations provide smooth curves between  $M_{R,CSM,y}$  and  $M_{R,CSM,z}$  and map surfaces that conform well to the numerical model surfaces.

$$\left[ \frac{M_y}{M_{R,CSM,y}} \right]^\alpha + \left[ \frac{M_z}{M_{R,CSM,z}} \right]^\beta \leq 1 \quad [18]$$

$$M_{R,CSM,y} = M_{CSM,y} (1 - n^{a_y})^{\frac{1}{b_y}} \quad [19]$$

$$M_{R,CSM,z} = M_{CSM,z} (1 - n^{a_z})^{\frac{1}{b_z}} \quad [20]$$

The powers  $\alpha$  and  $\beta$  are all defined in *Table 4* the tabulated powers were found via a non-linear least squares fitting regime, and are based on the ratio of the cross-section web area to gross area  $a = \frac{A_w}{A}$  and the ratio of the major to minor axis plastic section moduli  $W_r = \frac{W_{pl,y}}{W_{pl,z}}$ . A strain ratio of 5 is required before the convergence of the powers for l-sections, compared to that of 3 needed for box sections. The powers  $a_y$ ,  $a_z$ ,  $b_y$ ,  $b_z$ ,  $\alpha$  and  $\beta$  are all unity when  $\epsilon_{CSM}/\epsilon_y < 3$ .

*Table 4. CSM design powers  $a_y$ ,  $a_z$ ,  $b_y$ ,  $b_z$ ,  $a$  and  $\beta$  for combined loading. Liew, A. and Gardner, L. (2015)*

	$3 \leq \frac{\epsilon_{CSM}}{\epsilon_y} < 5$	$5 \leq \frac{\epsilon_{CSM}}{\epsilon_y} \leq 15$
	I-sections	
$a_y$		$a + 1.2$
$b_y$		0.8
$a_z$	2	$8a + 1.2$
$b_z$	1	$0.8 - 0.5a$
$\alpha$	$2 - 1.5n \geq 1$	$2 + 0.15W_r - 5n^{1.5} \geq 1.3$
$\beta$	$0.8 + 5n^{2.2} \leq 4$	$0.8 + (15 - W_r)n^{2.2} \leq 8$

## 2.4. Previous experimental programs

Eccentric compression test in major or minor axis has been conducted on stainless steel beam columns through different experimental programmes during the last decades, *Table 5* shows some of the previous studies where the

most of them were tested on RHS, SHS and lipped channels profiles and only two cases of I Welded profiles Burgan (2000) and Baofeng Zheng (2014). No information about combined loading was found as a previous reference in stainless steel.

Table 5. Test conducted on stainless steel beam columns

Date	Author	Material	Section	Number of Specimens	Type of test
1994	Hyttinen	1.4302 (304)	SHS	9	Transverse load + concentric compression
		1.4512 (409)	SHS	6	
		1.4003	SHS	6	
1995	Talja	304	SHS	4	Eccentric compression
			RHS	8	
2000	Burgan	1.4541 (312)	CHS	4	Eccentric compression Eccentric compression Major axis
		1.4435 (316L)	CHS	4	
		1.4301 (394)	Welded H	8	
2000	Rhodes	304	Lipped channel	22	Eccentric compression Minor axis (lip in tension)
2007	McDonald	304	Lipped channel	20	Eccentric compression Minor axis (lip in
2014	Fan	304	Lipped channel	38	Eccentric compression Major axis
2014	Huang	1.416	SHS	37	Eccentric compression
2014	Liu	2.205	SHS	20	Eccentric compression
2014	Gardner	Different Steels	Welded I		Combined loading
2014	Baofeng Zheng	304	SHS	5	Eccentric compression Major axis
			Welded H	5	

Nevertheless, Liew, A. and Gardner, L. (2015) has developed an extension of The Continuous Strength Method (CSM) to enable the prediction of the ultimate cross-section resistance of structural steel I-sections and box sections under combined loading (Table 6), where shows that CSM a strain based in structural steel design approach which allows for the beneficial influence of strain hardening. The applicability of the method to stainless steel structures was assessed by Theofanous et al. (2014).

Table 6. Test conducted on stainless steel RHS and SHS members subjected to compression and combined loading

Stainless Steel	Date	Author	Material	Number of Specimens	Type of test
Austenitic	1993a	Rasmussen and Hancock	1.4307	4	Flexural buckling
	1995	Talja and Salmi	1.4301	12	
	2003	Liu and Young	1.4301	12	
	2003	Young and Liu	1.4301	24	
	2004b	Gardner and Nethercot	1.4301	22	
	2006	Gardner et al.	1.4318	12	

As previous described, biaxial loading in stainless steel is an area that has remained relatively unexplored. Validation and analysis of stainless steel I welded cross-sectional resistance under biaxial loading is therefore the subject of the present study.

## Chapter 3

### NUMERICAL MODELLING

A numerical modelling programme was performed using the general-purpose finite element analysis package ABAQUS CAE. The objectives of the numerical investigations were firstly to reproduce part of the experimental data test results conducted by Baofeng Zheng (2015) at The Key Laboratory of C & PC Structures of Ministry of Education, Southeast University, Nanjing, China.

The column-beam experiment test was replicated with the aim of comparing the load-deformation histories obtained from tests with those derived from the numerical simulations. Finding accuracy of the load-deformation histories will let us to assess the sensitivity of the FE models to various input parameter to conduct parametric studies to generate further structural performance data over a wide range of I welded cross-section behavior under eccentric loading.

#### 3.1. Experimental Data

Zheng B., Hua X. and Shu G. (2015) undertook an experimental programme aiming to study the behavior of stainless steel beam-columns of welded I sections of austenitic stainless steel, subjected to eccentric load in the major axis, including material test, stub column test and beam-column test, with the aim of computing strengths of the specimens and comparing with Eurocode and American code predictions for stainless steel structures.

Tensile coupon test for welded I section were cut from web and flanges, using spark cutting machine. Coupon dimensions were established according to the

Chinese Standard GB/T 228.1 (2010). Test results were processed according to Equation [8], and described in chapter 2. Table 7 shows material properties obtained from coupon tensile test.

Table 7. Material properties obtained from coupon tensile test

Coupon	$E_o$ [Mpa]	$\sigma_{0.2}$ [Mpa]	$\sigma_{1.0}$ [Mpa]	$\sigma_u$ [Mpa]	$\epsilon_{t 0.2}$	$\epsilon_{t 1.0}$	$n$	$n_{0.2,1.0}$	$\delta$
HW-1	206551	244.10	306.45	694.97	0.00318	0.01148	3.50	2.90	66%
HW-2	195404	223.25	304.46	703.82	0.00307	0.01147	3.33	3.90	63%
HW-3	212338	238.27	311.37	656.47	0.00312	0.01147	2.45	3.60	68%
HF-1	199206	249.94	308.58	700.90	0.00325	0.01155	4.09	2.40	67%
HF-2	214003	257.37	325.52	683.81	0.00320	0.01152	3.48	2.80	57%
HF-3	209615	246.81	303.35	674.60	0.00318	0.01145	4.55	2.40	59%
Avg.	206186	243.29	309.96	685.76	0.00317	0.01149	3.57	3.00	63%

The experimental beam-column tests were tested in a 5000 kN hydraulic long column testing machine between pin-ended supports. Compression force was applied with a nominal eccentricity of 20 mm. Welded specimens were tested with free rotation about the major axis. To provide pin-ended supports, hinges were installed at each end of the specimens. The distance between the axis of the hinge and the top surface of the loading plate was measured to be 115 mm. Strain gauges were attached in the axial direction at mid-height of the specimens to determine the real loading eccentricity and local buckling (Figure 8).



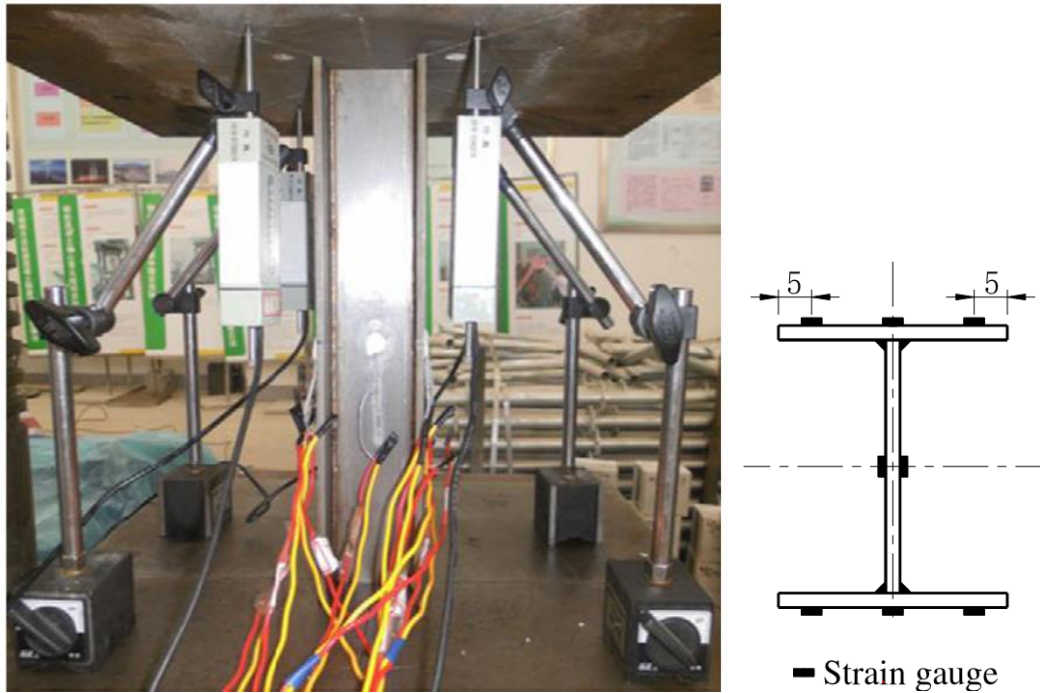


Figure 8. Stub column test setup and position of the strain gauges. Zheng B (2015)

Load-displacement response was obtained using a skew jack on the top of the loading plate of the hydraulic test machine; ultimate load is show in *Table 8*.

Table 8. Test results beam column specimens

Specimen	Fu [kN]	Le [mm]	er [mm]
80H1500	198.80	1730	17.00
80H2000	143.40	2230	13.50
80H2500	123.75	2729	20.25
80H3000	95.25	3230	16.93
80H3500	76.20	3730	16.61

The austenitic stainless steel 304 welded I beam-columns were tested between pin-ended supports to study cross sectional response. Table 9 shows measured dimensions and imperfections of I welded specimens.

Table 9. Measured dimensions and imperfections for welded H specimens.

Specimen	Dimension [mm]					Imperfection [mm]	
	h	b	tf	tw	L	e1	e2
80H1500	79.89	79.89	5.88	5.82	1499	1.00	0.50
80H2000	79.81	79.81	5.81	5.82	2000	0.00	1.50
80H2500	80.31	80.31	6.22	6.08	2499	0.50	0.50
80H3000	79.73	79.73	5.81	5.85	3000	0.50	0.50
80H3500	79.82	79.82	5.78	5.98	3496	0.25	1.58

### 3.2. Constitutive material equation

In order to obtain the most realistic engineering stress-strain curve, two different constitutive material equations for stainless steel were analysed, the one proposed by Eq [3] at EN-1993-1-4 (2006) and the one given by the experimental study [8].

Material properties used are shown in Table 10 and Table 11 for each case of study. The fundamental differences between case I and II data are based on the fact that EN-1993-1-4 formulae show values of  $n$  equal to 7, while the model experiment reduces that value by 50%. Similarly, strain hardening exponent corresponding to the second stage  $n_{0.2,1.0}$  has values of 30% of  $m$ .

Table 10. Case I: EN-1993-1-4 formulae

Coupon	$E_0$ [Mpa]	$\sigma_{0.2}$ [Mpa]	$\sigma_{1.0}$ [Mpa]	$\sigma_u$ [Mpa]	$\epsilon_{t0.2}$	$\epsilon_{t1.0}$	$n$	$m$	$E_y$ [Mpa]	$\epsilon_u$
HF-1	199206	249.9	308.6	700.9	0.003	0.012	7	4.814	16384	0.643
HF-2	214003	257.4	325.5	683.8	0.003	0.012	7	5.081	16929	0.624
HF-3	209615	246.8	303.4	674.6	0.003	0.011	7	4.939	16262	0.634
Avg.	206186	243.3	310	685.8	0.003	0.011	7	4.789	16027	0.645

Table 11. Case II: Experiment formulae

Coupon	$E_0$ [Mpa]	$\sigma_{0.2}$ [Mpa]	$\sigma_{1.0}$ [Mpa]	$\sigma_u$ [Mpa]	$\epsilon_{t0.2}$	$\epsilon_{t1.0}$	$n$	$n_{0.2,1.0}$	$\delta$	$E_{0.2}$ [Mpa]
HF-1	199206	249.94	308.58	700.9	0.003	0.012	4.09	2.4	67%	26492
HF-2	214003	257.37	325.52	683.81	0.003	0.012	3.48	2.8	57%	31530
HF-3	209615	246.81	303.35	674.6	0.003	0.011	4.55	2.4	59%	24015
Avg.	206186	243.29	309.96	685.76	0.003	0.011	3.57	3	63%	29242

Most materials that exhibit ductile behavior yield at stress levels that are orders of magnitude less than the elastic modulus of the material, which implies that the relevant stress and strain measures must be converted into true stress-strains to find more accuracy in result when simulation codes are used. For that, a true stress-strain material properties are input data required by ABAQUS, engineering stresses and strains were modified as  $\varepsilon_t = \ln(1 + \varepsilon)$  and  $\sigma_t = \sigma(1 + \varepsilon)$ . Figure 9 and Figure 10 shows true and engineering stress-strain curves for both constitutive equations in which is observed (true stress-strain curves) how the material can carry more load even with a reduction in cross-sectional area. The stress will continue to increase with strain as long as the strain hardening can compensate for this reduction in area.

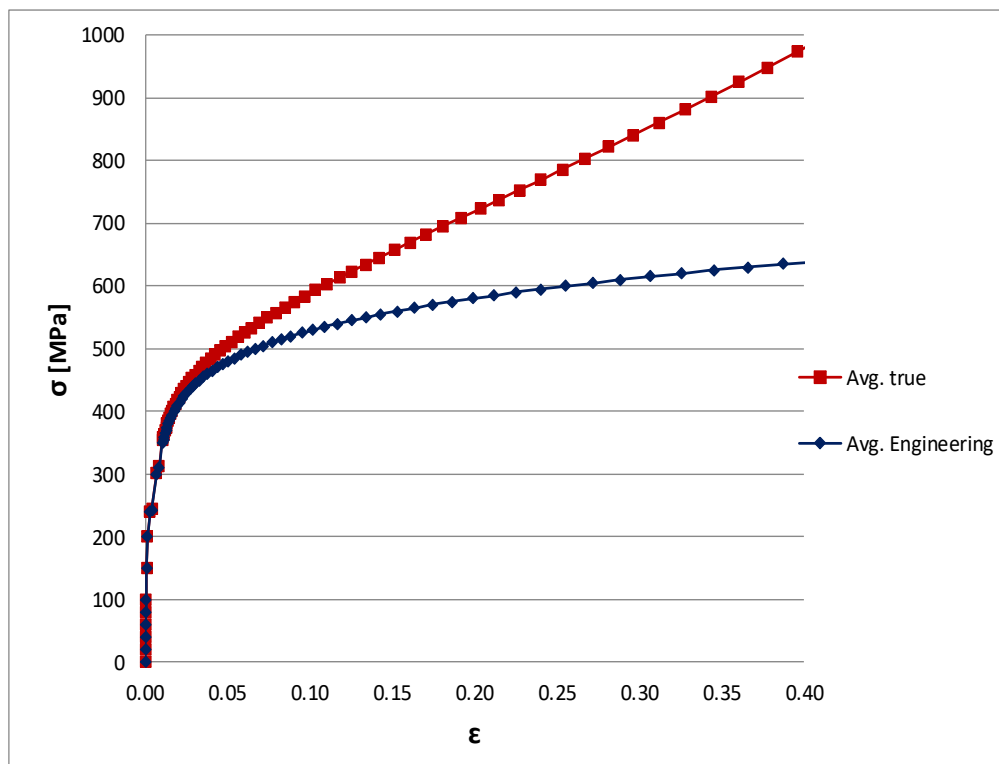


Figure 9. Engineering and true Stress-Strain curves according to EN-1993-1-4.

It is possible to observe that with the strain hardening exponent equals to 7 (Figure 8), for less strain we will have a nominal stress higher. But with strain hardening exponent equals to 3 for more strain nominal stress is smaller (Figure 9).

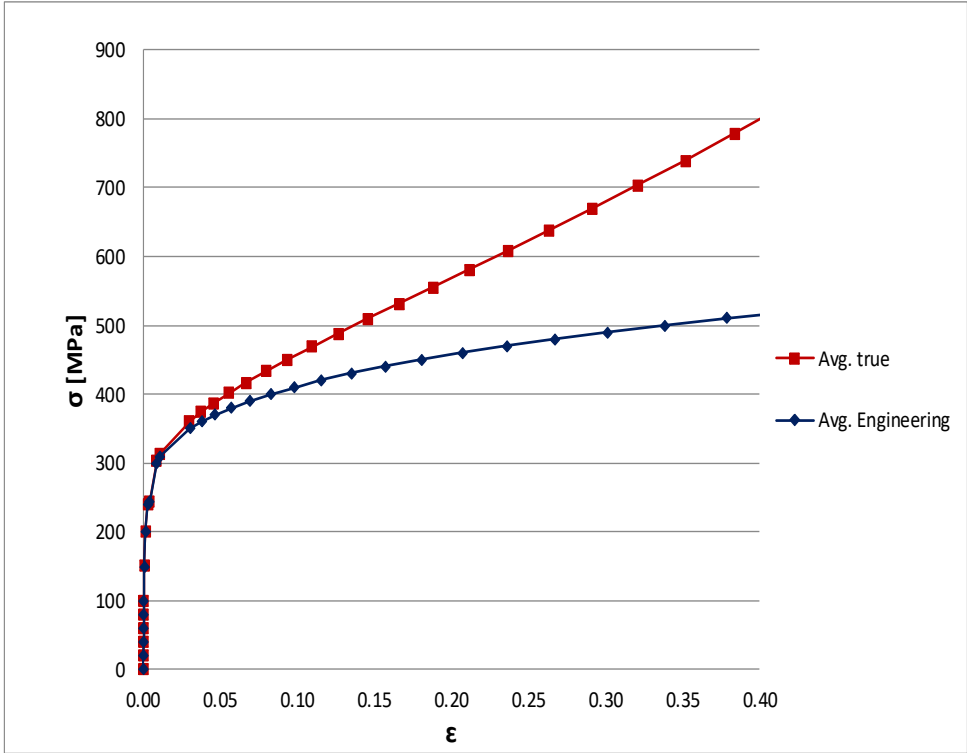


Figure 10. Engineering and true Stress-Strain curves according to Experiment.

Specimens: 80H1500, 80H2500, 80H3000 were analysed comparing Ultimate load response between equation [3] and [8], (Table 12), where ratios between equations indicates that there is no representative variation that influences in the use one or another equations although strain stresses curves have different behaviour, due to the fact that for small values of strain (less than 0.2), stresses in both cases reach similar values.

Table 12. Material properties sensitivity by ABAQUS.

Specimen	EN-1993-1-4	B. Zheng (2015)	Fu, EN/ Fu,B.Z
	Formulae	Formulae	
	Fu[Kn]	Fu [Kn]	
80H1500	280490	278826	1.006
80H2500	192584	187432	1.027
80H3000	108297	106633	1.016

Figure 10 shows a visual comparison of failure modes using different stress-strain curves, reaffirming that , equation given by EN-1993-1-4 (2006) allows higher values of stresses but it does not influence in the failure modes.

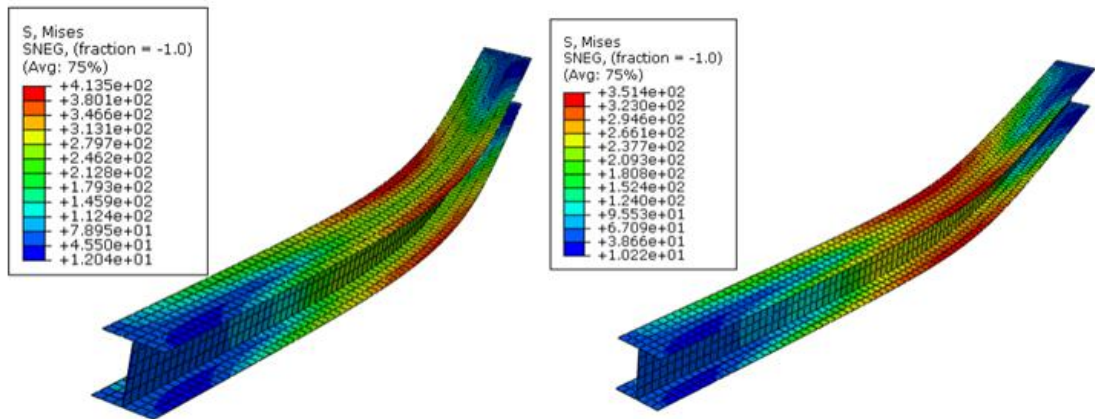


Figure 11. Ultimate Stresses according to EN-1993-1-4 and Experiment formulae.

For practical assumptions, equation given by EN-1993-1-4 (2006) was used for further development of the parametric study.

### 3.3. Basic modelling assumptions

Once verified accuracy of material response, modelling assumptions for all the input parameters considered in the experiment were also validated.

The four-node doubly curved shell element with reduced integration and finite membrane strain, S4R (ABAQUS) was designated as the element type to be used in the present study, which has been shown to perform well in similar studies : Gardner and Nethercot, (2004b) ; Ashraf et al., (2006a) ; and Arrayago et al., (2015).

Despite the fact that residual stresses are also introduced into the specimens during the production and their influence on structural members is to cause early yielding and loss of stiffness, resulting in reduced ultimate load-carrying capacity process, in the modelling assumptions residual stresses are not included, basing on recommendations of Becque J. and Rasmussen K.J.R. (2008) (2009c) which concluded that the magnitude of the membrane residual stresses is small compared to that of the bending residual stresses.

The end section boundary conditions were set considering free rotation about the major axis for both nodes, while, in order to study end shortening free displacement about longitudinal axils was allowed for Node 1.

Constraints applied at the end section were a surface-based coupling constraint which provides coupling between a reference node and a group of nodes referred to as the “coupling surface” this option provides the kinematic coupling constraint function and the distributing coupling elements with a surface-based user interface. The coupling nodes defined as a node-base slave surface were selected automatically at the end of each element, (Figure 12) named +RP1 and +RP2 respectively, located at the center of gravity of the cross-section.

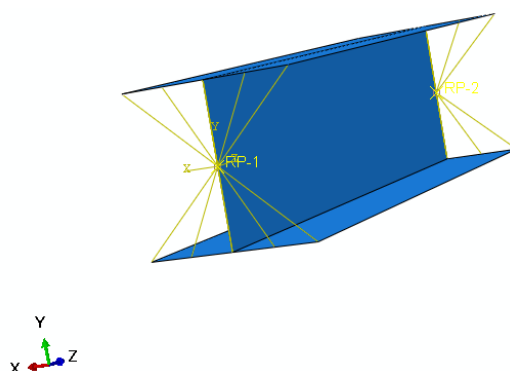


Figure 12. Coupling constraint at +RP1 and +RP2

Local imperfections can significantly influence stability response although are not relevant in stub columns and beams since cross-section failure is expected. These were incorporated into all FE specimens as the shape of the first local buckling mode, which was determined carrying out a prior elastic eigenvalue buckling analysis. Keeping in mind that eigenmodes represent the most dangerous shapes of imperfections (Dubina et al., 2001).

Geometrically and materially nonlinear analyses were performed, using the modified Riks method (ABAQUS) to trace the full load-deformation response of the specimens, including the post-ultimate path, where Imperfection amplitudes were taken equal to  $L/1500$  considering in the numerical analyses conducted by Arrayago et al, (2015).

### 3.4. Model validation

The accuracy of the FE models was assessed by comparing the ultimate loads obtained by Abaqus with the experiment results. Results are shown in Table 13.

Table 13. Test and Abaqus results of 80H specimens

Specimen	B. Zheng	Abaqus	Ratio
	Fu [kN]	Fu [kN]	
80H1500	198.8	210.12	1.06
80H2500	123.75	128.75	1.04
80H3000	95.25	118.54	1.24

The difference between Ultimate loads obtained by Zheng B., Hua X. and Shu G. (2015). experiment and the obtained by Abaqus are significantly high. The reason may be attached to the fact that residual stresses weren't considered. The residual stress has a little effect on the ultimate load capacity of stainless steel welded I-section beams, where the lack of residual stress consideration, increase value of Ultimate load, this may be a fact that influences in the relatively high values of difference between experimental data and test results.

### 3.5. Conclusion remarks

The ratios obtained between Abaqus and experiment results are a little bit above from unity but not too far. The performance of the FE model has been demonstrated to be an adequate tool to reproduce the behaviour of I welded sections loaded in compression.

It has been showed that it is possible to adopt it as a template to study the behaviour of I welded cross section under eccentric loading conditions.

It must be taken into account that possible variations on theoretical and Abaqus results may be found due a lack of consideration of residual stresses.





## Chapter 4

### PARAMETRIC STUDY

Once numerical modelling was validated, it was used as a template to carry out a parametric study related to the variation of load application point coordinates and alfa and beta exponents values. These parametric studies were performed to generate and gather the results of multiple analyses that differ only in the values of some of the parameters used in place of input quantities.

Five lengths 100, 200, 250, 350 y 500 mm specimens were defined following modelling assumptions defined in chapter 3. Elastic critical force  $N_{cr}$  was obtained as the first eigenvalue mode from buckle analysis, to further calculate non dimensional slenderness as a function of length [15] (Table 14)

Table 14. Non slenderness values related to length.

I	II	III	IV	V
L=100 $\lambda=0.230$	L=200 $\lambda=0.269$	L=250 $\lambda=0.283$	L=300 $\lambda=0.287$	L=400 $\lambda=0.490$

#### 4.1. Parametric study on Load application point.

In order to assess design expression given in EN-1993-1-4 for stainless steel cross-sections under eccentric loading a parametric study was carried out using Python subroutines, recognized by Abaqus efficiently.

It was focus on a variation of the load application point, ranging their coordinates on a radial form from 0 to 359 degrees with different eccentricity values in order to analyze behavior of members subjected to accidentals eccentricities which is a common mistake during construction procedures.

Load application point was varied radially, considering the center of gravity as a datum of the cross section profile. For this purpose, radius and angle (eccentricity and thita) vectors were defined in the subroutine, which were varied between 5, 20, 30 and 40mm and 0 to 359 degrees respectively, thus generating 1440 samples. (Figure 13). Values of eccentricity where taken from 5 to 40mm to evaluate critical points were 5mm is not too far from non-eccentric loading, 20-30mm could be considered as a medium eccentricity and 40mm as maximum eccentricity to avoid been outside section plane.

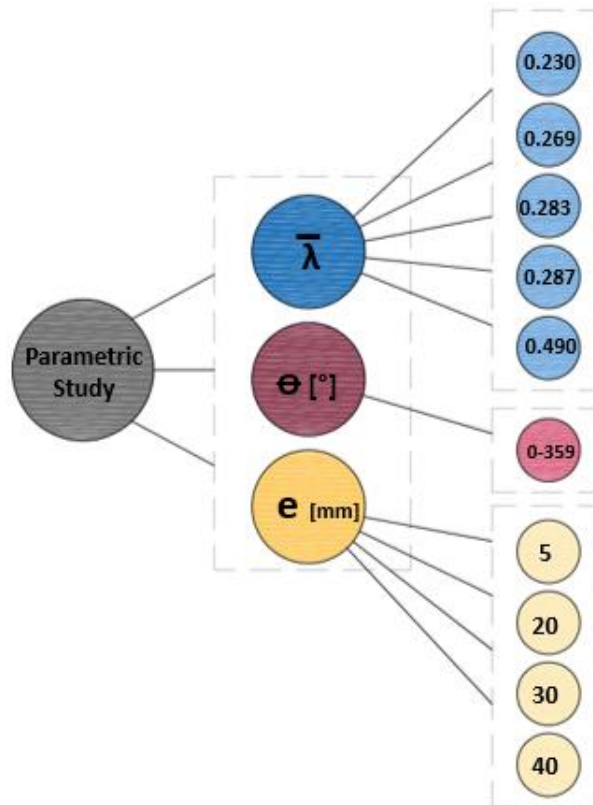


Figure 13. Parametric study variables and combinatorics.

Modelling assumptions are shown in (Figure 14), major and minor axis, trigonometric functions used to defined coordinates of load application points and upper right quadrant.

Throughout the numerical study, problem symmetry was used to simplify calculations. Using the circumference upper right quadrant, where sine and cosine values are positive for angles from 0 to 90 degrees.

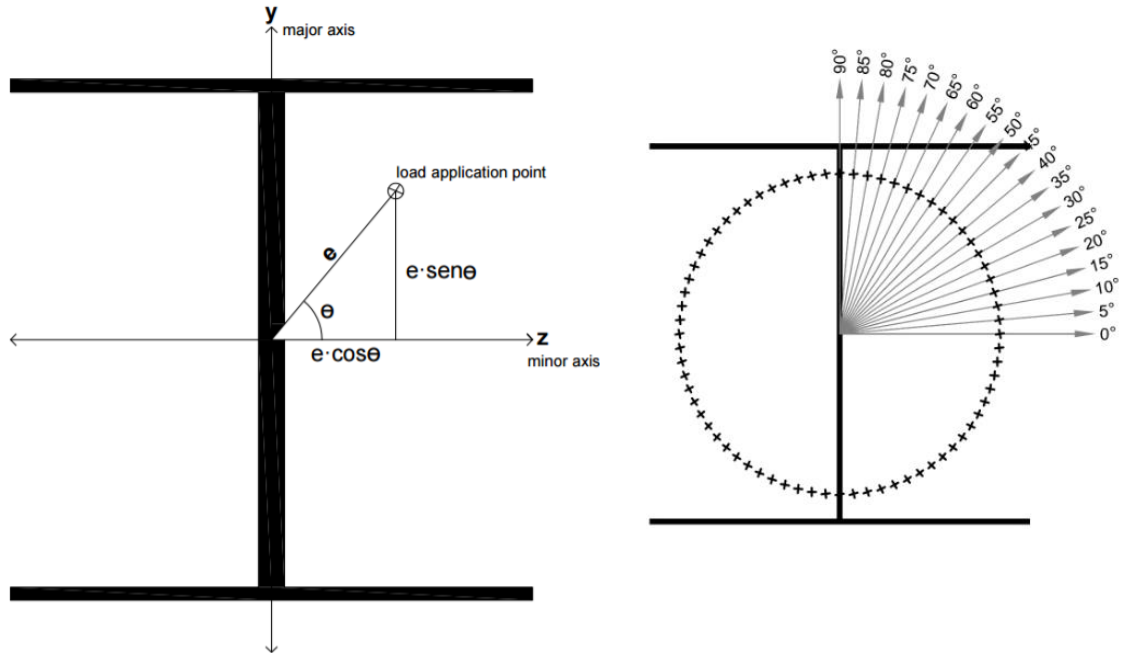


Figure 14. Modelling assumptions.

This study generates a high computational cost, due to the large number of element that must be included in the process to find accuracy of results, to reduce use of computer memory, ultimate load ratios between consecutive angles were compared and results variations start being representative with increments of 5 degrees, for that subroutine was modified and subsequences specimens were discretized using angles increments every 5 degrees (Figure 15).

```

sbnolinealH80_100.psf * x
parameter = ParStudy (par=('tita','e'),name='nolineal80_100_EN')
parameter.define(CONTINUOUS, par='tita', domain=(0,6.2657))
parameter.define(CONTINUOUS, par='e', domain=(0,20))
valores_tita = (0.0,0.087,0.175,0.262,0.349,0.436,0.524,
0.611,0.698,0.785,0.873,0.960,1.047,1.134,1.222,1.309,1.396,1.484,1.571
)
valores_e = (5,20,30,40)
parameter.sample(VALUEES, par='tita', values=valores_tita)
parameter.sample(VALUEES, par='e', values=valores_e)
parameter.combine(MESH)
parameter.generate(template='nolineal80_100_EN')
parameter.execute(ALL)
import odbAccess

```

Figure 15. Python simplified subroutine.

Results of a representative single case are shown in (Table 15) where maximum load values are highlighted for each case. Loads and displacements values obtained from the parametric study corresponding to “ $e=20\text{mm}$ ,  $\theta=5^\circ$ ” sample. Load values are the reaction force obtained from Node 2 (+PR2) and displacements to the longitudinal displacements at Node 1 (load application point), results are ordered from minor to major increment (0-100) reached in the non-linear analysis.

The maximum load values corresponding to all points of the sample were gathered in Table 16 with increments between angles of 5 in 5 to further analyzed ratios between numerical and theoretical results.

## Chapter 4 Parametric Study

Table 15. Load-Displacements values of a representative single case  $e=20\text{mm}$ ,  $\theta=5^\circ$ .

e= 20mm, $\theta= 5^\circ$										
Increment	L=100		L=200		L=250		L=300		L=500	
	Load [kN]	Displacement [mm]	Load [kN]	Displacement [mm]	Load [kN]	Displacement [mm]	Load [kN]	Displacement [mm]	Load [kN]	Displacement [mm]
1	0.00	0.000	0.00	0.000	0.00	0.000	0.00	0.000	0.00	0.000
2	15.00	0.005	5.00	0.005	13.99	0.016	5.00	0.008	1.40	0.003
3	30.00	0.010	10.00	0.010	27.97	0.033	9.99	0.016	2.80	0.007
4	52.50	0.018	17.49	0.017	48.91	0.058	17.47	0.029	4.90	0.011
5	86.26	0.030	28.73	0.027	80.27	0.094	28.68	0.047	8.04	0.019
6	136.11	0.047	45.59	0.043	127.17	0.151	45.44	0.075	12.74	0.030
7	175.78	0.073	70.84	0.067	177.74	0.242	70.50	0.116	19.78	0.046
8	202.25	0.117	108.68	0.104	205.55	0.323	107.88	0.177	30.31	0.071
9	222.03	0.156	159.64	0.164	222.74	0.408	156.62	0.274	46.00	0.108
10	234.67	0.194	190.21	0.222	232.01	0.499	184.32	0.362	69.36	0.163
11	241.69	0.231	211.34	0.279	239.14	0.588	203.17	0.443	103.97	0.244
12	247.33	0.267	229.70	0.369	247.84	0.714	220.64	0.572	149.93	0.369
13	252.20	0.322	239.28	0.464	259.05	0.888	230.24	0.716	176.22	0.481
14	258.71	0.403	247.01	0.552	268.72	1.054	237.32	0.853	193.73	0.580
15	267.51	0.525	257.05	0.676	277.16	1.217	243.10	0.979	206.57	0.680
16	279.55	0.706	270.48	0.852	284.74	1.379	250.70	1.152	215.29	0.788
17	295.08	0.897	282.13	1.024	291.66	1.541	260.21	1.397	221.36	0.902
18	314.46	1.092	292.18	1.196	298.05	1.703	268.26	1.634	225.88	1.018
19	339.33	1.380	301.07	1.370	303.95	1.866	275.19	1.866	231.11	1.183
20	362.56	1.785	309.22	1.542	312.06	2.111	284.09	2.214	235.12	1.337
21	383.14	2.157	320.43	1.800	319.45	2.353	291.49	2.563	238.49	1.478
22	407.78	2.491	335.41	2.180	326.25	2.591	297.61	2.909	242.78	1.675
23	424.60	2.795	350.62	2.616	332.49	2.826	302.85	3.245	246.42	1.862
24	434.76	3.078	363.40	3.046	338.20	3.059	307.43	3.573	249.55	2.043
25	440.36	3.346	373.92	3.471	343.42	3.291	311.41	3.897	252.29	2.220
26	442.88	3.413	382.14	3.887	348.17	3.520	314.78	4.217	255.04	2.421
27	443.15	3.480	387.73	4.296	352.47	3.748	317.63	4.533	257.33	2.621
28	443.21	3.578	390.46	4.694	356.30	3.974	319.97	4.846	259.24	2.818
29	443.26	3.725	390.78	4.793	359.64	4.198	322.57	5.309	260.88	3.011
30	443.31	3.872	391.00	4.891	362.48	4.421	324.27	5.766	262.28	3.201
31	443.36	4.018	391.06	5.037	364.75	4.641	325.19	6.218	263.44	3.389
32	443.35	4.166	390.83	5.182	366.44	4.858	325.32	6.331	264.38	3.576
33	443.16	4.387	390.33	5.325	367.50	5.072	325.42	6.443	265.08	3.762
34	442.55	4.609	389.08	5.539	367.92	5.280	325.49	6.612	265.52	3.947
35	441.08	4.829	386.09	5.854	367.70	5.483	325.44	6.780	265.78	4.131
36	439.23	5.050	382.22	6.168	366.88	5.679	325.28	6.946	266.00	4.316
37	437.12	5.274	377.94	6.480	365.51	5.869	324.96	7.108	266.12	4.500
38	434.89	5.584	372.74	6.850	363.64	6.052	324.45	7.266	266.15	4.685
39	431.34	5.898	367.68	7.221	361.32	6.229	323.79	7.421	266.14	4.870
40	427.69	6.214	362.80	7.592	357.00	6.484	322.98	7.574	266.05	5.055
41	423.72	6.534	358.09	7.963	351.75	6.729	322.03	7.726	265.86	5.240
42	419.50	6.858	353.39	8.327	345.85	6.969	320.92	7.878	265.58	5.425
43	415.24	7.185	348.78	8.688	339.66	7.207	318.95	8.102	265.23	5.609
44	411.02	7.515	344.31	9.049	333.41	7.446	315.21	8.435	264.68	5.787
45	406.85	7.847	339.96	9.409	327.26	7.686	310.47	8.761	263.84	5.957
46	402.75	8.181	335.77	9.769	321.28	7.928	304.78	9.085	262.81	6.123
47	398.66	8.517	331.56	10.129	315.47	8.172	298.26	9.408	261.67	6.286
48	394.59	8.858	327.38	10.488	307.05	8.541	291.14	9.733	260.51	6.450
49	390.58	9.202	323.25	10.847	298.98	8.916	283.64	10.063	259.33	6.615

51	382.72	9.901	315.25	11.564	283.76	9.686	268.06	10.737	256.90	6.947
52	378.89	10.257	311.38	11.922	276.78	10.080	260.59	11.081	255.59	7.114
53	375.13	10.615	307.62	12.278	267.01	10.682	253.50	11.431	254.20	7.280
54	371.45	10.977	303.98	12.634	257.96	11.299	246.81	11.787	252.77	7.448
55	367.86	11.343	300.42	12.988	249.51	11.930	240.54	12.149	251.31	7.616
56	364.36	11.712	296.97	13.341	241.60	12.575	234.64	12.517	249.80	7.786
57	360.95	12.084	293.61	13.691	234.22	13.234	227.09	13.031	248.26	7.956
58	357.62	12.457	290.34	14.039	227.32	13.907	220.10	13.555	246.72	8.128
59	354.36	12.832	287.14	14.384	220.86	14.593	213.56	14.090	245.14	8.301
60	351.16	13.210	284.02	14.727	214.80	15.294	207.42	14.635	243.55	8.477
61	348.03	13.591	280.96	15.068	209.07	16.009	201.63	15.192	241.96	8.654
62	344.98	13.974	277.96	15.407	203.66	16.738	196.15	15.760	240.35	8.832
63	341.99	14.359	275.00	15.744	198.54	17.482	190.84	16.341	238.72	9.012
64	339.06	14.747	272.10	16.080	193.67	18.239	185.79	16.933	237.07	9.195
65	336.19	15.138	269.23	16.415	189.04	19.011	181.03	17.536	235.41	9.379
66	333.37	15.533	266.42	16.750	184.63	19.797	176.56	18.150	233.73	9.566
67	330.61	15.930	263.65	17.084	180.41	20.598	172.33	18.775	232.03	9.755
68	327.91	16.330	260.92	17.420	176.39	21.413	168.34	19.412	230.33	9.947
69	325.25	16.734	258.24	17.756	172.54	22.242	164.56	20.060	228.64	10.141
70	322.65	17.140	255.60	18.092	168.86	23.086	160.97	20.718	226.92	10.337
71	320.10	17.549	253.01	18.430	165.33	23.943	157.55	21.388	225.18	10.537
72	317.60	17.962	250.44	18.770	161.94	24.816	154.28	22.069	223.41	10.740
73	315.15	18.377	247.92	19.111	158.67	25.702	151.17	22.761	221.58	10.945
74	312.74	18.796	245.43	19.454	155.53	26.602	148.18	23.464	219.66	11.154
75	310.39	19.218	243.00	19.798	152.49	27.515	145.31	24.176	217.63	11.367
76	308.09	19.643	240.62	20.146	149.57	28.444	142.56	24.899	215.50	11.583
77	305.83	20.071	238.29	20.495	146.74	29.385	139.91	25.633	213.26	11.803
78	303.62	20.501	236.01	20.847	144.01	30.340	137.36	26.376	210.89	12.027
79	301.45	20.935	233.77	21.200	141.37	31.309	134.90	27.130	208.43	12.254
80	299.33	21.371	231.58	21.557	138.80	32.293	132.53	27.894	205.88	12.484
81	297.26	21.810	229.43	21.915	136.32	33.290	130.25	28.667	203.25	12.716
82	295.22	22.251	227.33	22.276	133.91	34.301	128.03	29.451	200.58	12.952
83	293.22	22.695	225.27	22.638	131.57	35.326	125.89	30.245	197.87	13.190
84	291.26	23.141	223.24	23.003	129.29	36.365	123.82	31.048	195.10	13.431
85	289.35	23.590	221.25	23.370	127.09	37.418	121.81	31.861	192.27	13.674
86	287.48	24.041	219.30	23.739	124.94	38.484	119.86	32.683	189.43	13.921
87	285.65	24.495	217.38	24.110	122.84	39.565	117.96	33.514	186.61	14.170
88	283.86	24.952	215.51	24.483	120.79	40.660	116.11	34.355	183.84	14.421
89	282.11	25.411	213.67	24.859	118.79	41.768	114.32	35.205	181.12	14.675
90	280.41	25.872	211.87	25.236	116.84	42.890	112.56	36.064	178.46	14.931
91	278.75	26.336	210.10	25.615	114.93	44.025	110.85	36.932	175.88	15.190
92	277.12	26.803	208.35	25.996	113.08	45.175	109.19	37.809	173.37	15.451
93	275.54	27.272	206.65	26.380	111.25	46.338	107.56	38.695	170.94	15.714
94	273.98	27.743	204.97	26.765	109.47	47.514	105.97	39.590	168.60	15.980
95	272.47	28.217	203.33	27.152	107.72	48.704	104.42	40.494	166.33	16.248
96	270.98	28.693	201.72	27.542	106.01	49.907	102.90	41.406	164.13	16.518
97	269.54	29.171	200.14	27.933	104.33	51.123	101.40	42.326	161.99	16.791
98	268.13	29.652	198.59	28.327	102.68	52.353	99.94	43.254	159.92	17.066
99	266.75	30.134	197.06	28.723	101.06	53.596	98.50	44.191	157.91	17.344
100	265.40	30.619	195.57	29.120	99.47	54.852	97.08	45.136	155.96	17.624

Load-displacements curves were plotted (Figure 16) to analyze in Chapter 5 the influence of varying load application point in terms of end-shortening and Ultimate load and to verify that the program physical response was in line with which what was expected.

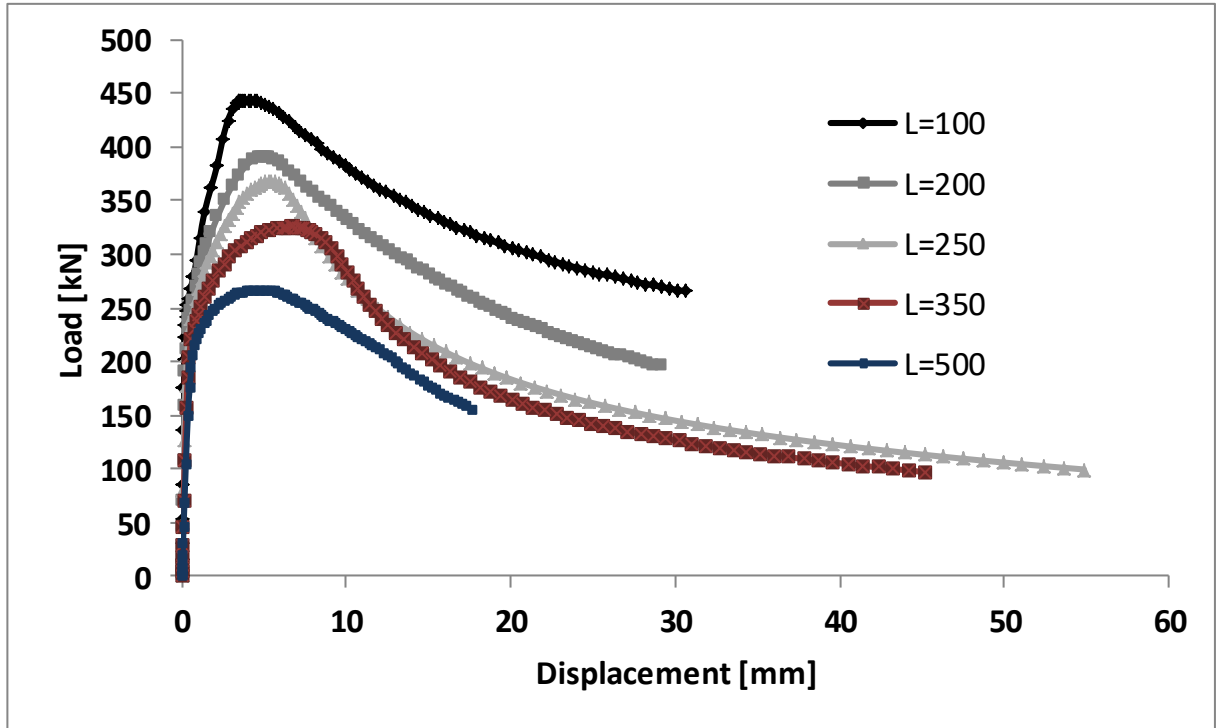


Figure 16. Load-Displacements curve of a representative case  $e=20\text{mm}$ ,  $\theta=5^\circ$ .

Table 16. Numerical results from Abaqus

THEORETICAL Results		NUMERICAL Results				
Angle	$\lambda < 0.2$ N <sub>Ed,EN</sub> [kN]	$\lambda = 0.2304$ N <sub>Ed,max</sub> [kN]	$\lambda = 0.2691$ N <sub>Ed,max</sub> [kN]	$\lambda = 0.283$ N <sub>Ed,max</sub> [kN]	$\lambda = 0.287$ N <sub>Ed,max</sub> [kN]	$\lambda = 0.49$ N <sub>Ed,max</sub> [kN]
0	317	442	390	367	325	266
5	317	443	391	368	325	266
10	318	446	393	370	327	267
15	320	453	397	373	329	269
20	323	458	401	378	333	272
25	326	464	408	383	338	276
30	331	471	416	390	344	280
35	336	480	425	399	351	286
40	343	491	437	408	360	293
45	350	504	449	420	370	302
50	359	515	461	432	381	311
55	370	534	475	444	393	321
60	382	547	489	459	407	331
65	396	565	507	472	420	340
70	412	582	525	489	435	351
75	430	605	541	503	451	361
80	448	629	556	519	467	374
85	462	659	581	539	482	389
90	466	689	621	590	500	404

#### 4.2. Parametric study on alpha and beta powers.

In order to reach one of the objectives proposed in this study, a sensitivity analysis of the maximum axial force applied on I welded cross sections,  $N_{Ed,max}$  was developed, varying values of alpha and beta powers.

An excel worksheet enabled for macros was used as a mathematical (*Figure 17*) tool to calculate the maximum applied load value resisted by the cross section for which the equation [12] quoted in chapter 2 is equal to unity.



Alpha	e [mm]	ez [mm]	ey [mm]	Mz,Ed [N-mm]	My,Ed [N-mm]	MN,z,Rd [N-mm]	MN,y,Rd [N-mm]	n	$\alpha$	$\beta$	Eq [12]	Ned [kN]
0	20	20.00	0.00	5278323	0	8353614	18476886	0.44	2	1	1.00	317
1	20	20.00	0.35	5277458	92118	8353614	18476886	0.44	2	1	1.00	317
2	20	19.99	0.70	5275621	184229	8353614	18476886	0.44	2	1	1.00	317
3	20	19.97	1.05	5272771	276334	8353614	18476886	0.44	2	1	1.00	317
4	20	19.95	1.40	5268903	368438	8353614	18476886	0.44	2	1	1.00	317
5	20	19.92	1.74	5264013	460541	8353614	18476886	0.44	2	1	1.00	317
6	20	19.89	2.09	5258094	552648	8353614	18476886	0.44	2	1	1.00	317
7	20	19.85	2.44	5251142	644759	8353614	18476886	0.44	2	1	1.00	317
8	20	19.81	2.78	5241217	736605	8353614	18476886	0.44	2	1	1.00	318
9	20	19.75	3.13	5231348	828564	8353614	18476886	0.44	2	1	1.00	318
10	20	19.70	3.47	5220307	920481	8353614	18476886	0.44	2	1	1.00	318
11	20	19.63	3.82	5208095	1012351	8353614	18476886	0.44	2	1	1.00	318
12	20	19.56	4.16	5194708	1104169	8353614	18476886	0.44	2	1	1.00	319
13	20	19.49	4.50	5180145	1195931	8353614	18476886	0.44	2	1	1.00	319
14	20	19.41	4.84	5164406	1287631	8353614	18476886	0.44	2	1	1.00	319
15	20	19.32	5.18	5147488	1379265	8353614	18476886	0.44	2	1	1.00	320
16	20	19.23	5.51	5129390	1470829	8353614	18476886	0.44	2	1	1.00	320
17	20	19.13	5.85	5110104	1562316	8353614	18476886	0.44	2	1	1.00	321
18	20	19.02	6.18	5089652	1653728	8353614	18476886	0.44	2	1	1.00	321
19	20	18.91	6.51	5068010	1745056	8353614	18476886	0.44	2	1	1.00	322
20	20	18.79	6.84	5045184	1836297	8353614	18476886	0.44	2	1	1.00	322
21	20	18.67	7.17	5022806	1928075	8353614	18476886	0.44	2	1	1.01	323
22	20	18.54	7.49	4997847	2019261	8353614	18476886	0.44	2	1	1.01	323
23	20	18.41	7.81	4971716	2110368	8353614	18476886	0.45	2	1	1.01	324
24	20	18.27	8.13	4944411	2201394	8353614	18476886	0.45	2	1	1.01	325
25	20	18.13	8.45	4915930	2292336	8353614	18476886	0.45	2	1	1.01	325
26	20	17.98	8.77	4886272	2383194	8353614	18476886	0.45	2	1	1.01	326
27	20	17.82	9.08	4855432	2473966	8353614	18476886	0.45	2	1	1.01	327
28	20	17.66	9.39	4823409	2564652	8353614	18476886	0.45	2	1	1.01	328
29	20	17.49	9.70	4790200	2655251	8353614	18476886	0.45	2	1	1.01	329
30	20	17.32	10.00	4755801	2745763	8353614	18476886	0.45	2	1	1.01	275

Figure 17. Excel worksheet used to compute Parametric Study on alfa and beta.

This tool was used for each case described in Table 17, where case I: alpha is assumed equal to unity and variations of beta are proposed; Case II alpha equal to two and variations of beta, generating from 8 cases of study, which will be compared with the two theoretical cases and in this way to contrast the convergence of the results and obtain samples that are close to the numerical results obtained from the calculation program. Table 18 shows the results obtained from the sensitivity study, for e=20mm which will be analyzed in the next chapter.

Table 17. Cases of study generated by Alfa and beta variations.

<b>Case</b>	<b><math>\alpha</math></b>	<b><math>\beta</math></b>
<b>I</b>	<b>1</b>	<b>1</b>
I.a	1	2n
I.b	1	3n
I.c	1	4n
I.d	1	5n
<b>II</b>	<b>2</b>	<b>5n</b>
II.a	2	1
II.b	2	2n
II.c	2	3n
II.d	2	4n

Table 18. Alfa and beta influence.

Angle	Case I					Case II				
	NEd $\alpha=1, \beta=1$ [kN]	NEd $\alpha=1, \beta=2n$ [kN]	NEd $\alpha=1, \beta=3n$ [kN]	NEd $\alpha=1, \beta=4n$ [kN]	NEd $\alpha=1, \beta=5n$ [kN]	NEd $\alpha=2, \beta=n$ [kN]	NEd $\alpha=2, \beta=2n$ [kN]	NEd $\alpha=2, \beta=3n$ [kN]	NEd $\alpha=2, \beta=4n$ [kN]	NEd $\alpha=2, \beta=5n$ [kN]
0	264	264	264	264	264	264	264	264	264	264
5	260	261	261	262	262	264	264	264	264	138
10	258	258	259	261	262	265	265	265	265	139
15	256	256	258	261	262	266	266	266	267	139
20	255	256	258	261	263	268	268	268	269	141
25	255	255	258	262	264	270	271	271	272	142
30	255	256	260	264	267	273	274	275	276	144
35	257	258	262	267	271	277	278	279	280	147
40	259	261	266	272	275	281	282	284	285	150
45	262	265	270	277	281	286	288	289	292	153
50	267	270	276	283	288	292	294	296	299	157
55	273	277	283	291	297	298	302	304	308	162
60	280	286	292	301	307	306	311	314	318	631
65	289	296	304	313	319	315	321	325	330	645
70	300	310	317	327	334	325	333	337	343	669
75	313	326	334	344	351	337	347	352	358	691
80	331	346	354	364	370	351	362	367	374	707
85	354	370	376	382	385	368	378	381	385	717
90	388	388	388	388	388	388	388	388	388	721

## **Chapter 5**

### **ANALYSIS OF RESULTS**

This chapter presents the numerical and theoretical results obtained from the parametric study described in chapter 4 with their respective analysis and discussions.

Basically, it is desired to show orientation images obtained from the calculation program that lead to know the phenomenological behavior of welded I profiles subjected to eccentric loading. Next, the results for ultimate loads subjected to a pure compression and that corresponding to the eccentric loading resulting from the variation of the load application point in a radial coordinates are presented.

In order to observe the results tendency obtained from the calculation program, some images shown the maximum load that resist the section as a function of the magnitude of the eccentricity and a variation of the angle of the most representative cases: pure compression, flexion around minor and major axis and biaxial bending for 5, 15, 30, 45, 60 and 75 degrees. Finally, the images corresponding to the sensitivity study of the alpha and beta coefficients are shown.

In this chapter, special emphasis is placed on the influence of considering material proof stress values similar to those considered in the calculation program.

## 5.1. Phenomenological Insight

In order to know the maximum stresses that resisted by the specimens, von Mises stresses were evaluated in profiles subjected to compression loading at the increment corresponding to maximum load.

Figure 18 shows L=500, 350, 250 and 200 mm profiles, where the value for which the element yields are  $\sigma_{0.2\%} = 467 \text{ N/mm}^2$ ,  $496 \text{ N/mm}^2$ ,  $486 \text{ N/mm}^2$  and  $489 \text{ N/mm}^2$  respectively.

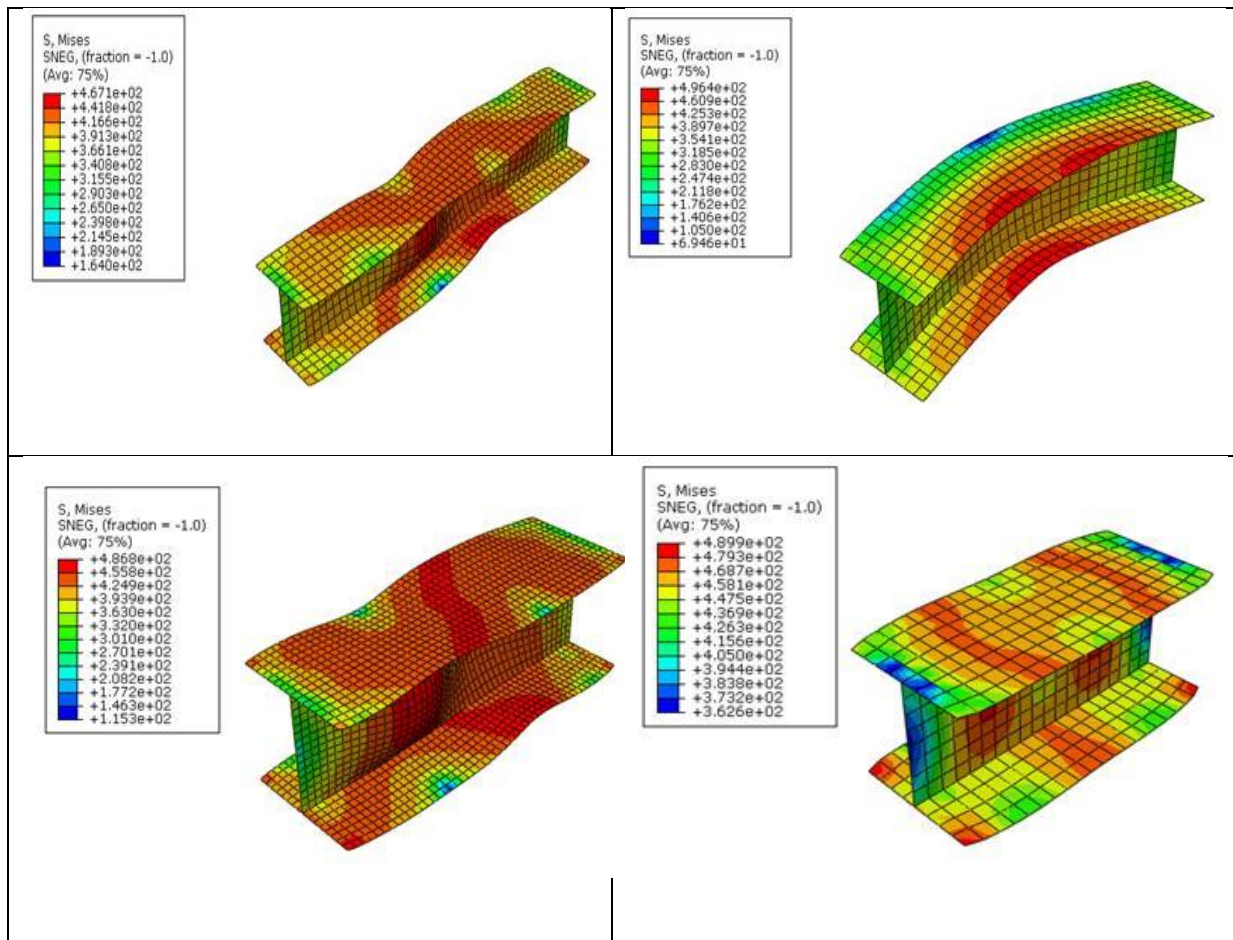


Figure 18. Von Mises stresses due to compression loading L=500-350-250-200.

Figures above indicates that numerical model reach higher values of stress than the ones assumed for the design code and it significantly under-estimate the structural response in terms of resistance of stainless steel I members subjected to compression loading, mainly owing to the lack of consideration for strain hardening.

To understand the structural behavior of stainless steel I welded profiles subjected to different load scenarios of eccentric loading, a brief summary of the images corresponding to the von Mises stresses of the studied profiles are shown (Figure 19-20) sequentially arranged according to the load application point.

The maximum stresses for L=250mm specimens (Table 19) between 0 and 45 degrees take values of 560 N/mm<sup>2</sup> and 575 N/mm<sup>2</sup>, while for 45 to 90 degrees, decrease but not in a representative way reaching values between 525 N/mm<sup>2</sup> and 533 N/mm<sup>2</sup>.

Table 19. Maximun Von Mises stresses for L=250mm

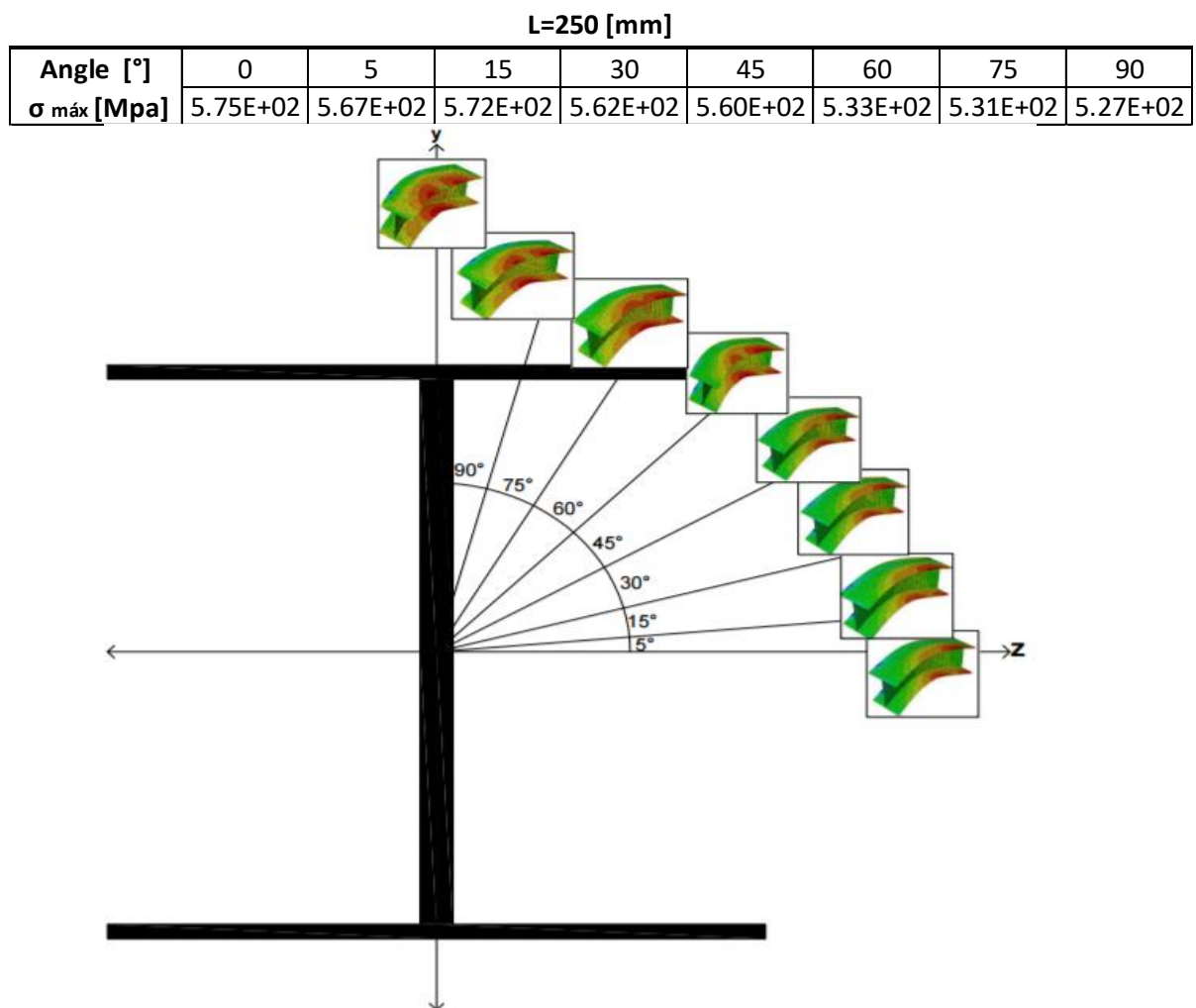


Figure 19. Structural response due to loading point ranging. L=250mm

A reduccion of stress due to increment of length is show in (Table 20). For L=350mm specimens stresses between 0 and 45 degrees take values of 492

$\text{N/mm}^2$  and  $500\text{N/mm}^2$ , while for 45 to 90 degrees, decrease but not in a representative way reaching values between  $339\text{N/mm}^2$  and  $492\text{ N/mm}^2$ .

Table 20. Maximun Von Mises stresses for  $L=350\text{mm}$

		<b>L=350 [mm]</b>							
<b>Angle [°]</b>	0	5	15	30	45	60	75	90	
<b><math>\sigma_{\text{máx}}</math> [Mpa]</b>	5.00E+02	5.16E+02	5.04E+02	4.90E+02	4.92E+02	4.83E+02	4.86E+02	3.39E+02	

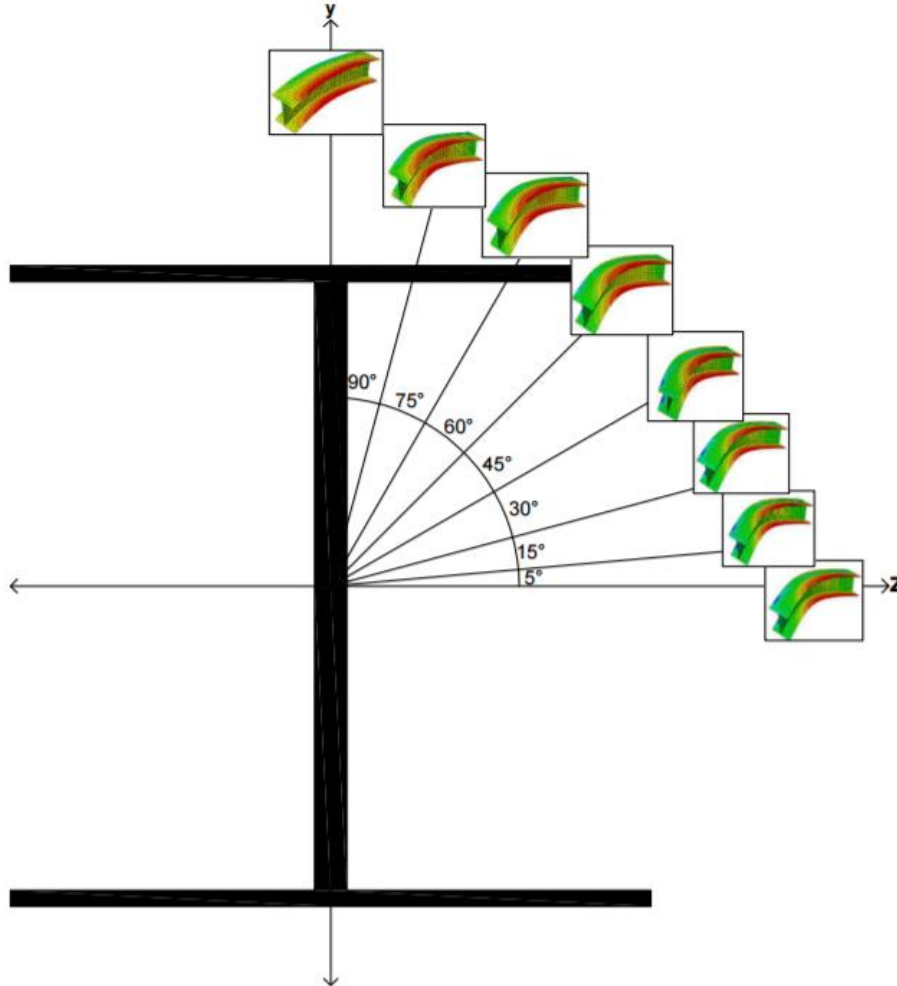


Figure 20. Structural response due to loading point ranging.  $L=350\text{mm}$

For profiles subjected to compression loads as well as those subjected to eccentric loading, there is a substantial increase in stainless steel strength, which exceeds the value obtained from the stress strain material response corresponding to  $\sigma_{0.2\%} = 243\text{ N/mm}^2$ .

## 5.2. Analysis of members subjected compression loading

Herein is detailed the physical response of members subjected to a buckle analysis with the application of a compression load equal to unity, noticing that numerical results corresponding to the elastic critical force corresponding to the eigenvalues associated with the first mode of buckling and theoretical values follow EN-1933-1-4 (2006) formulae.

Theoretical results, show very low values of non-dimensional slenderness compared to numerical values, (*Table 21*) and it is attach to the fact that calculation program considers a value of elastic limit above the  $\sigma_{0.2\%}$  recommended by the code.

On the other hand, elastic critical force  $N_{cr}$  take similar values when length element is higher than 250mm, due to the failure mode is different from global buckling.

For samples of very low slenderness (length less than 250mm) a lack of sensitivity to the simulation program to initial imperfections in stub columns may be also attached.

Table 21. Non-dimensional slenderness and elastic critical force.

L	Theoretical results by EN-1993-14		Numerical results by Abaqus		Variation	
	N <sub>cr</sub> [kN]	$\bar{\lambda}_{EN}$	N <sub>cr</sub> [kN]	$\bar{\lambda}_{num}$	$\bar{\lambda}_{num}/\bar{\lambda}_{Theor}$	$N_{cr,num}/N_{cr,Theor}$
100	33897	0.10	6155	0.23	2.35	0.18
200	8474	0.20	4513	0.27	1.37	0.53
250	5423	0.25	4067	0.28	1.15	0.75
350	2767	0.34	2764	0.34	1.00	1.00
500	1355	0.49	1302	0.50	1.02	0.96

Finally, Table 22 shows the theoretical and numerical values of reduction factor  $\chi$ . For Lengths higher than 250mm reduction factor of both cases take similar values, nevertheless for stub columns (L=100 y L=200mm) the scatter between theoretical and numerical results, is remarkable since the design code underestimate cross sectional resistance.

Table 22. Theoretical and numerical values of reduction factor  $\chi$ .

L[mm]	Theoretical results by EN-1993-14			Numerical results by Abaqus		
	$\bar{\lambda}_{EN}$	$\phi_{,EN}$	$\chi_{,EN}$	$\bar{\lambda}_{num}$	$\phi_{,num}$	$\chi_{,num}$
100	0.098	0.466	<b>1.085</b>	0.230	0.538	0.976
200	0.196	0.518	<b>1.003</b>	0.269	0.563	0.947
250	0.246	0.547	<b>0.965</b>	0.284	0.572	0.936
350	0.344	0.614	<b>0.891</b>	0.344	0.614	0.891
500	0.491	0.731	<b>0.786</b>	0.501	0.740	0.779



Figure 21 helps to understand that calculation program reproduce more realistic results than code predictions, since local buckle is observed for both members which verify accuracy of results.

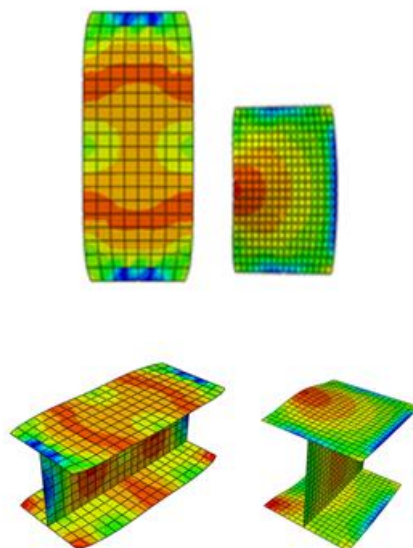


Figure 21. Local Buckling L=100 and L=200 mm.

Finally, in Figure 22 the plots were based on EN-1993-1-4(2006) terminology and numerical model results in which the reduction factor  $\chi$  is plotted against non-dimensional slenderness  $\bar{\lambda}$ . Points corresponding to  $L=100_{,Abaqus}$ ,  $L=200_{,Abaqus}$  still being at the buckle zone, which mean that avoiding reduction factor values generates out of safety results.

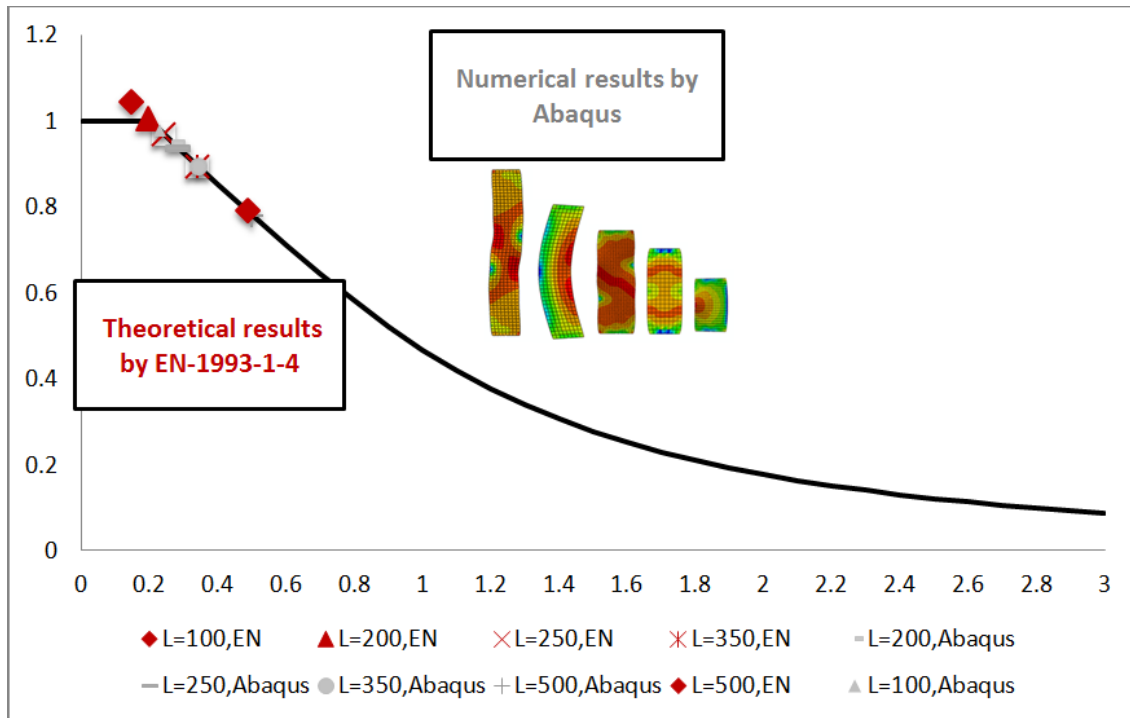


Figure 22. Theoretical and numerical results reduction factor  $X$ .

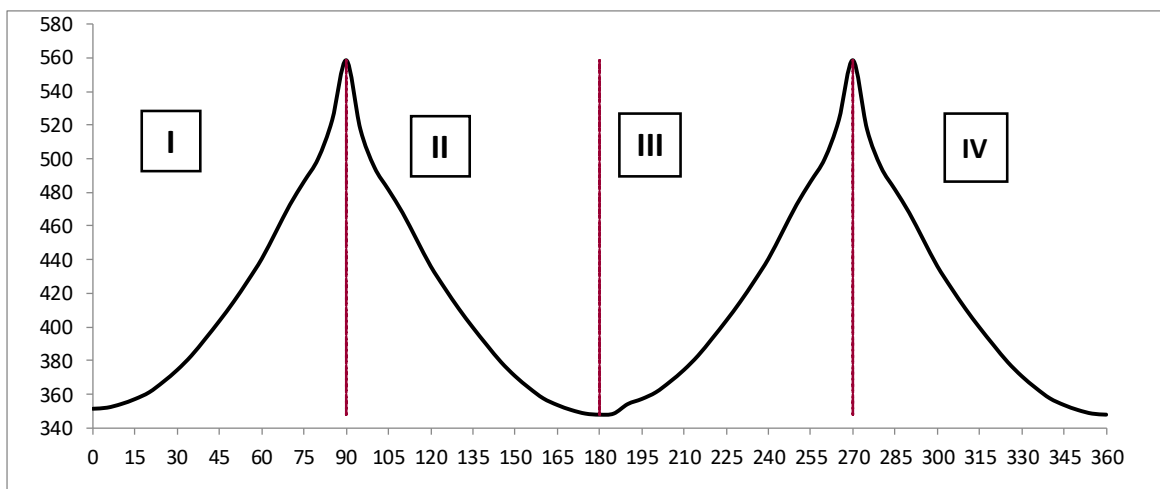
As described in chapter 4, values of sigma corresponding to the ultimate load were found. Table 23 shows how numerical model display lower deformations for each case of study and in consequence higher values of stress and plastic load resistance. Therefore it is suggested to evaluate the criteria recommended by EN-1993-1-4 (2006) for resistance calculations of stainless steel profiles, since there is an increase in strength that is not being considered.

Table 23. Influence of  $\sigma_{0.2\%}$  according to EN-1993-1-4 and Abaqus.

Specimen	Theoretical results			Numerical Results			$N_{pl,EN} / N_{pl,num}$
	$\sigma_{0.2\%,EN}$	$\epsilon_{0.2\%}$	$N_{pl,EN}$ [kN]	$\epsilon_{num}$	$\sigma_{U,num}$	$N_{pl,num}$ [kN]	
H80_100			327	0.033	465	626	1.91
H80_200			327	0.026	447	601	1.84
H80_250	243	0.004	327	0.024	435	585	1.79
H80_350			327	0.017	418	563	1.72
H80_500			327	0.020	402	540	1.65

### 5.3. Analysis of members subjected eccentric loading

The expected physical response of cross sections under biaxial bending is shown in *Figure 23*, whereby subjecting them to radial variations between 0 and 360 degrees, a symmetrical behavior of the piece is observed every 45 degrees. As expected, the lower capacity occurs when load is applied near to the minor axis: 0-45 degrees and the higher sectional resistance occurs in the areas where load application point is close to the section major axis: 45-90 degrees.



*Figure 23. Cross sectional behavior subjected to eccentric loading around from 0 to 360 degrees.*

#### 5.3.1. Influence of variation of load application point

Due to the high computational requirements related to time and computer memory, parametric study is focused only on the first part of the curve shown in *Figure 23*, obtaining results from 0 to 90 degrees that can easily mirroring for the following parts by their symmetrical behavior.

*Figure 24* shows magnitude eccentricity influence on non-slender elements, for 5 mm eccentricities, which the response has a similar behavior to the case of compression loading. For greater eccentricities, a reduction of  $N_{Ed,max}$  due to presence of biaxial moment occurs.

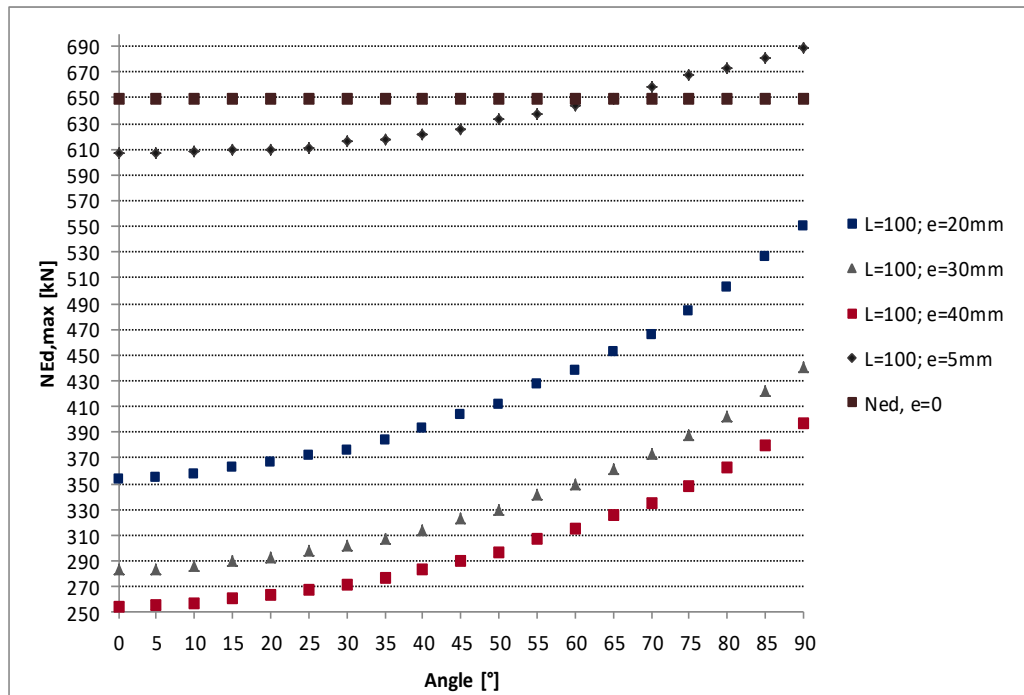


Figure 24. Influence of magnitude and angle variation,  $L=100$ mm.

In Figure 25 is observed that from 65 to 90 degrees all curves begin to have a similar behavior and loss of load-bending capacity is no longer observed. Also curves corresponding to  $e=30$  and  $40$  mm has the same behavior and values of  $N_{Ed}$ .

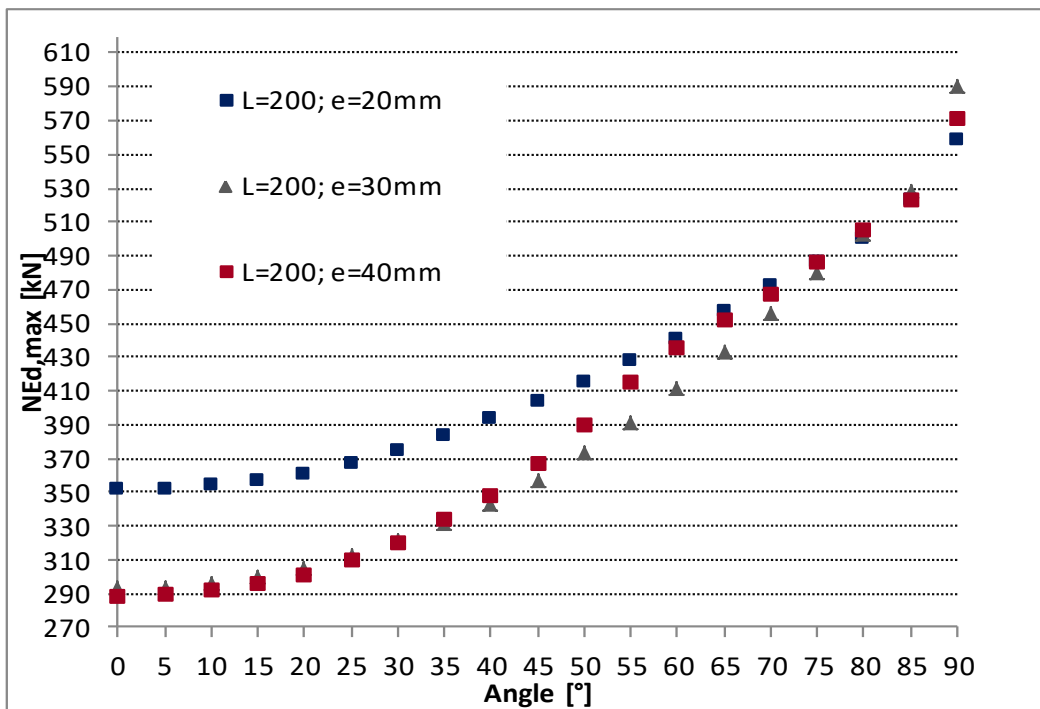


Figure 25. Influence of magnitude and angle variation,  $L=200$ mm.

As specimen's length increases, eccentricity magnitude influence decreases in the area close to the major axis: 70 to 90 degrees (Figure 26).

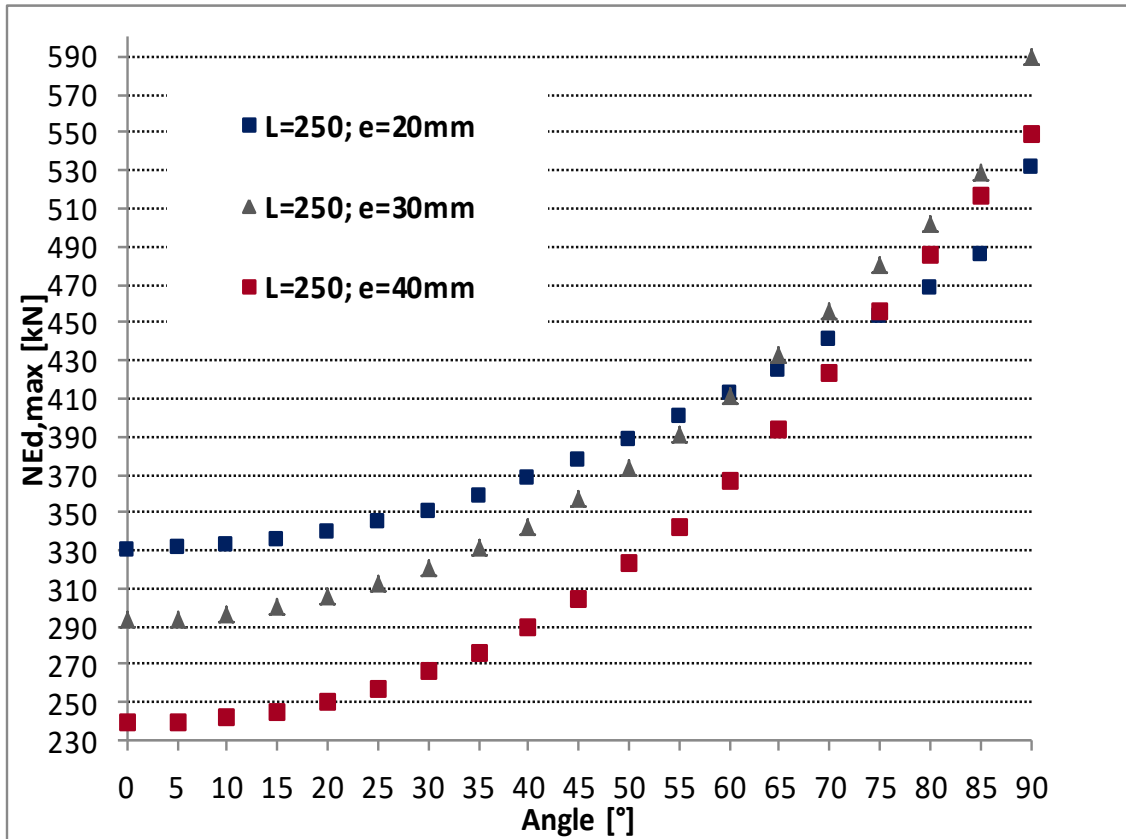


Figure 26. Influence of magnitude and angle variation, L=250mm.

Reduction of  $N_{Ed,max}$  due to the presence of moment is no longer observed between 55 and 70 degrees for 30 and 40mm eccentricity (Figure 27).

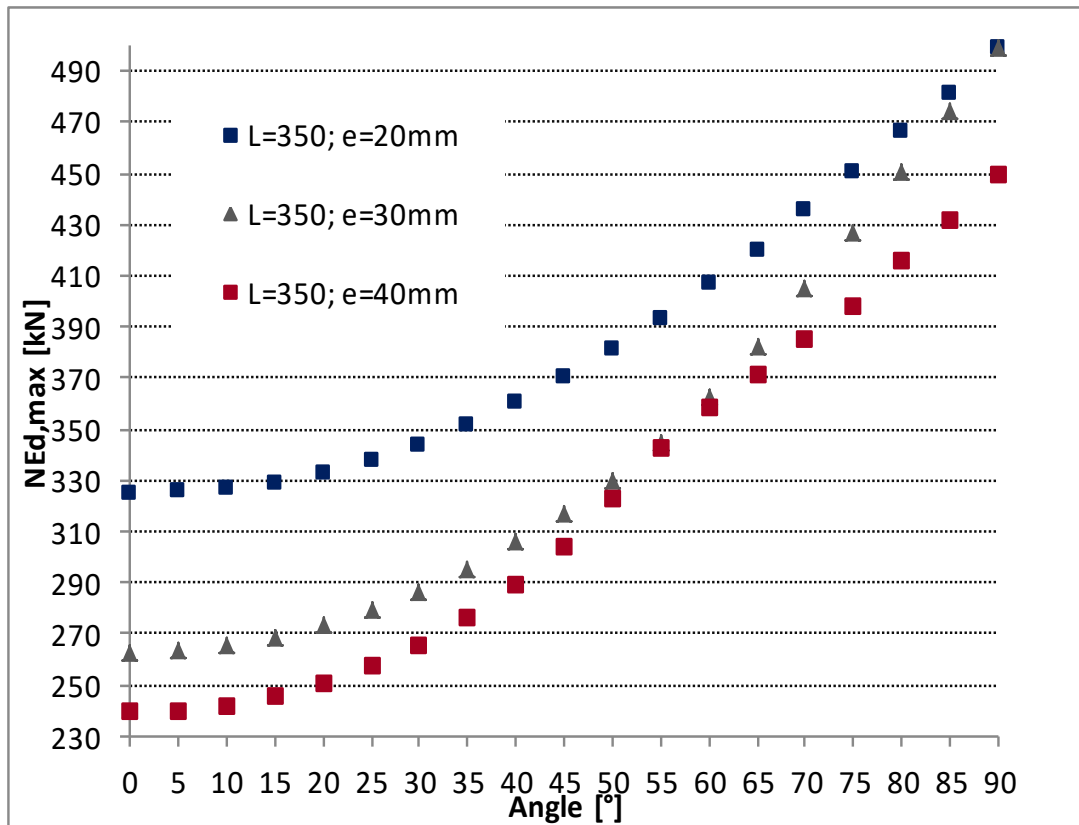


Figure 27. Influence of magnitude and angle variation, L=350mm.

For greater eccentricities and lengths, loss of load capacity  $N_{Ed,max}$  due bending moment occurs, it may be attributed to the presence of global instability (Figure 28). Particularly, in this case magnitude eccentricity influence is similar from 0 to 80 degrees. Between 80 and 90 degrees loss of axial load is not affected by eccentricity magnitude.

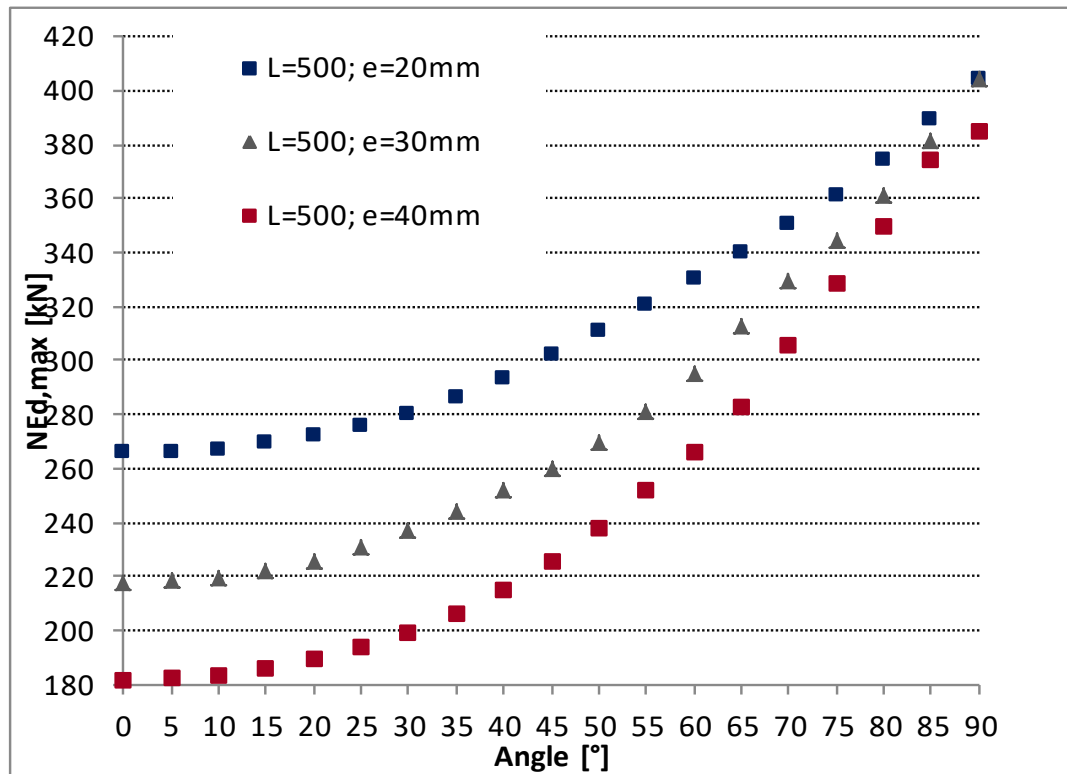


Figure 28. Influence of magnitude and angle variation, L=500mm.

From the figures above it is concluded that the safety zone (angles for which the eccentricity magnitude stop influencing) decreases as the length of the element increases.

With the previous images it is verified that Abaqus shows a quite correct physical representation of the phenomenon of study and also recognizes the parametric variation of eccentricity as a function of the angle and magnitude.

The axial-moment interaction of the piece as a function of the applied eccentricity is shown in *Figure 29*, taking as reference and equal to one a line which represents compression profiles behavior. For 5 mm eccentricities, axial load is reduced with ranges from 5 to 13 percent for all angles, which indicates that in the case of smaller eccentricities, axial reduction due to eccentricity is not representative.

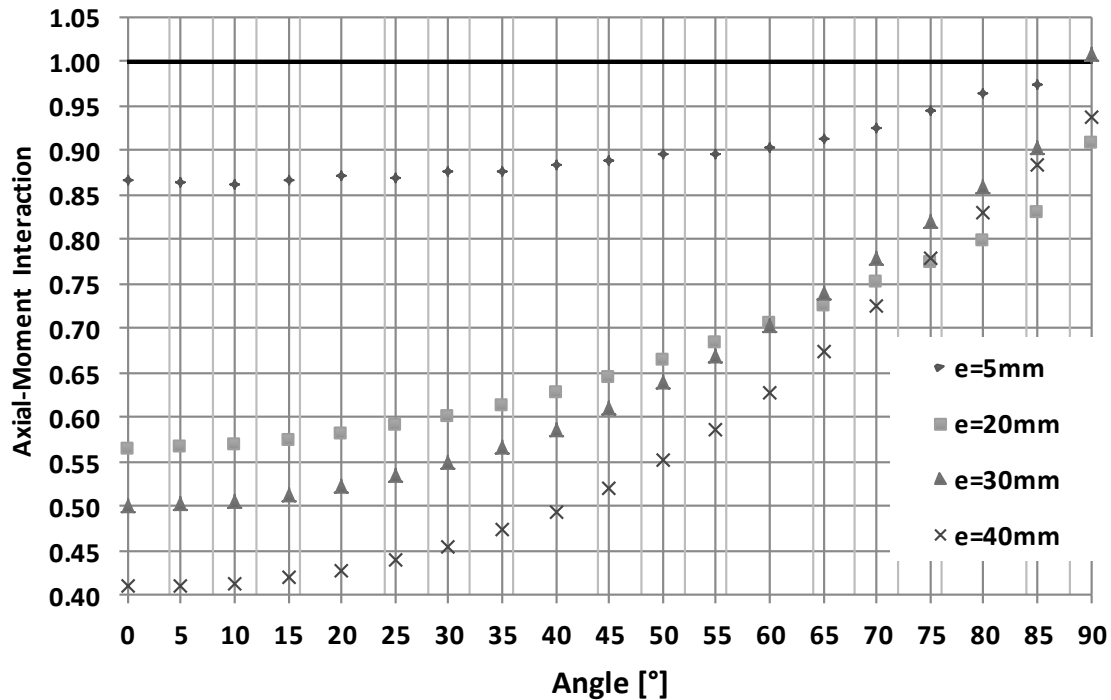


Figure 29. Axial-Moment interaction.

Conversely, when eccentricity takes values of 20, 30 and 40 mm, plastic resistance reduction produced by the axial-moment interaction increases by five percent for each magnitude of eccentricity at angles between 0 and 45 degrees, while between 45 and 90 degrees axial reduction has less scatter despite variation in the magnitude of the eccentricity.

Finally, in Table 24 ratio between numerical and theoretical axial load results in the length function is shown. For smaller lengths, the code underestimates biaxial bending resistance of I sections between 25 and 30 percent. This confirms the conservative criteria adopted by the normative related to ultimate cross sectional capacity of I welded stainless steel profiles.

Figure 30 shows that the more conservative cases of study are between 30-70 degrees. Higher values of load resistance in function of angle variation are presented by 5 to 10 percent.

Finally, L=500mm specimen results cannot be considered as representative due the presence of global instability phenomena.



Table 24. Theoretical and numerical response

Angle	$N_{Ed,L=100}/N_{Ed,EN}$	$N_{Ed,L=200}/N_{Ed,EN}$	$N_{Ed,L=250}/N_{Ed,EN}$	$N_{Ed,L=350}/N_{Ed,EN}$	$N_{Ed,L=500}/N_{Ed,EN}$
0	1.34	1.33	1.25	1.23	1.01
5	1.34	1.33	1.25	1.23	1.01
10	1.35	1.34	1.25	1.23	1.01
15	1.36	1.34	1.26	1.23	1.01
20	1.36	1.34	1.26	1.24	1.01
25	1.36	1.35	1.27	1.24	1.01
30	1.36	1.36	1.27	1.24	1.02
35	1.37	1.36	1.28	1.25	1.02
40	1.37	1.37	1.28	1.26	1.02
45	1.37	1.38	1.29	1.26	1.03
50	1.37	1.38	1.29	1.27	1.03
55	1.38	1.38	1.29	1.27	1.03
60	1.36	1.37	1.29	1.27	1.03
65	1.36	1.37	1.28	1.26	1.02
70	1.34	1.36	1.27	1.25	1.01
75	1.33	1.34	1.25	1.24	1.00
80	1.33	1.32	1.24	1.24	0.99
85	1.36	1.35	1.25	1.24	1.01
90	1.42	1.44	1.37	1.29	1.04

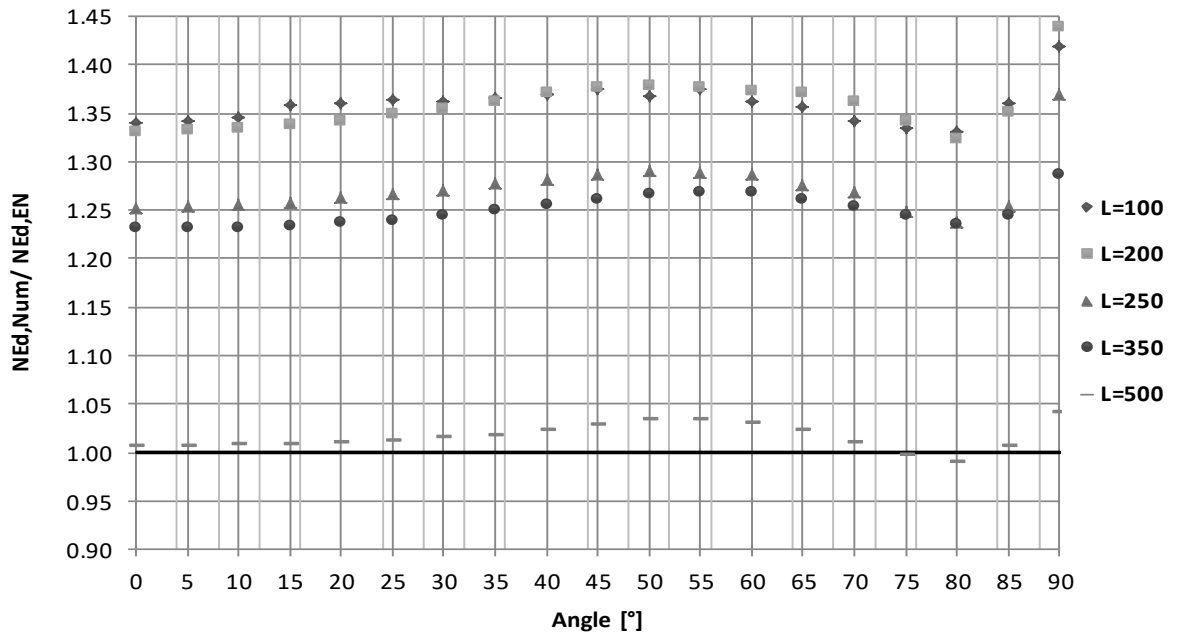


Figure 30. Theoretical and numerical results.

### 5.3.2. Alpha and beta Analysis

For all eccentricities values studied, if recommendation of EN-1993-1-4 (2006) is followed, where alpha and beta exponents can be taken, conservatively equal to the unit, a significant loss of  $N_{Ed,max}$  (values greater than 10 percent) is generated between 30 and 85 degrees.

Table 25 shows loads for the cases of study and the reduction ratios between Abaqus and the code criteria, Figure 31 helps to understand the described phenomenon, where it clearly shows the axial reduction according to the values that take alpha and beta.

Table 25. Reduction of  $N_{Ed,max}$  due to alpha and beta exponents

Angle	$N_{Ed,num}$ [kN]	$N_{Ed, \alpha=2, \beta=2n}$ [kN]	$N_{Ed, \alpha=1, \beta=1}$ [kN]	$N_{Ed,num} / N_{Ed, \alpha=2, \beta=2n}$	$N_{Ed,num} / N_{Ed, \alpha=1, \beta=1}$
0	266	264	264	1.01	1.01
5	266	264	260	1.01	1.02
10	267	265	258	1.01	1.04
15	269	267	256	1.01	1.05
20	272	269	255	1.01	1.07
25	276	272	255	1.01	1.08
30	280	276	255	1.02	1.10
35	286	281	257	1.02	1.11
40	293	287	259	1.02	1.13
45	302	293	262	1.03	1.15
50	311	301	267	1.03	1.17
55	321	310	273	1.03	1.18
60	331	321	280	1.03	1.18
65	340	333	289	1.02	1.18
70	351	347	300	1.01	1.17
75	361	363	313	1.00	1.15
80	374	378	331	0.99	1.13
85	389	387	354	1.01	1.10
90	404	388	388	1.04	1.04

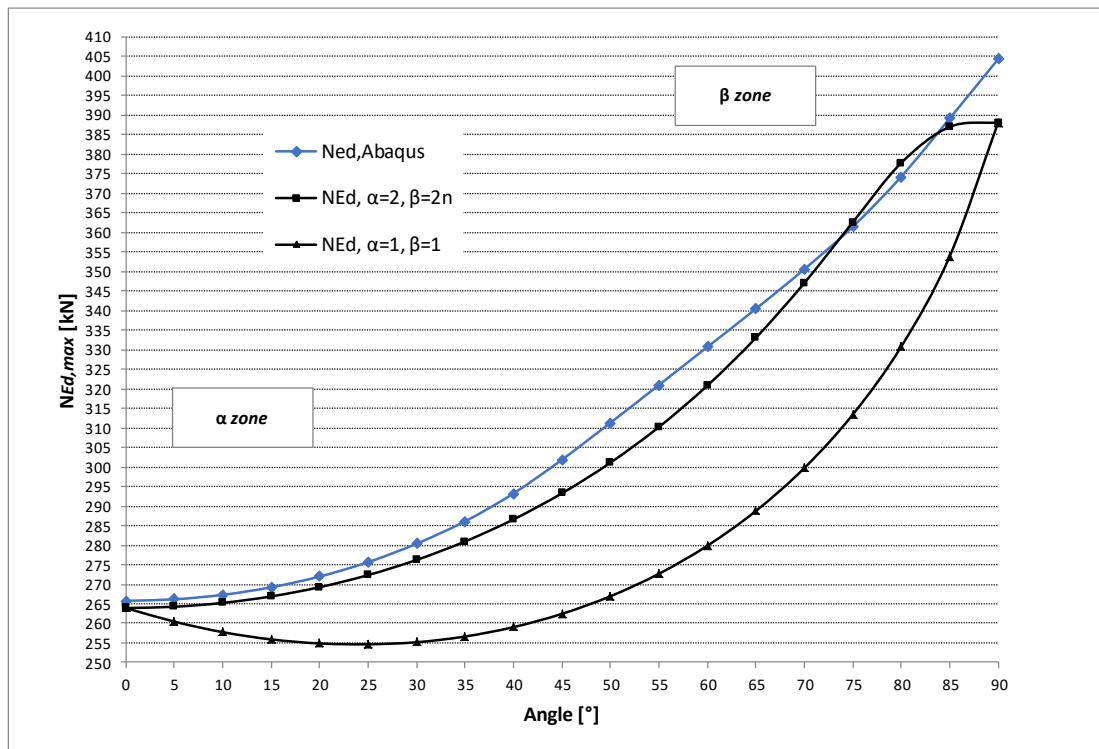


Figure 31. Reduction of  $N_{Ed,max}$  due to  $\alpha$  and  $\beta$  exponents.

On the basis of all of the above, it is stated that, using the exponents related to the conservative form  $\alpha$  and  $\beta$  equal to the unit, is not efficient from the point of view of sectional resistance.

The criterion proposed by Liew, A. and Gardner, L. (2015) and shown in *Table 4* recommended that  $\alpha$  and  $\beta$  can be taken equal to the unit if, the strain ratio complies with the relation  $\frac{\epsilon_{cms}}{\epsilon_y} < 3$ .  $\epsilon_{cms}$  is the deformation equivalent to the ultimate load mentioned in previous chapters and  $\epsilon$  is the strain corresponding to  $\sigma_{0.2\%}$ .

*Table 26* shows the strain ratios for all specimens studied with lengths 100, 200, 250, 350 and 500 mm is greater than 3, while, for samples with lengths greater than 1500, the ratio decreases.

To assume  $\alpha$  and  $\beta$  less than unity, deformation ratio should be compute in advance or, for profiles subjected to eccentric loading such as those studied in the present work, lengths must be greater than 1500mm to avoid Gardner criterion.

Table 26. Verification of Strain ratio of members

Modelo	L [mm]	$\epsilon_{0,2\%} = \epsilon_y$	$\epsilon_{f(du)} = \epsilon_{CSM}$	$\epsilon_{CSM} / \epsilon_y$
H80_100	100		0.0334	7.9231
H80_200	200		0.0262	6.2237
H80_250	250		0.0239	5.6782
H80_350	350	0.0042	0.0167	3.9706
H80_500	500		0.0199	4.7167
H801500	1500		0.0014	0.3294
H802500	2500		0.0075	1.7888

#### 5.4.1. Sensitivity analysis to alpha and beta

In order to contrast EN-1993-1-4 (2006) and Liew, A. and Gardner, L. (2015) and to generate less conservative and more realistic proposals, a sensitivity analysis of the maximum axial applied  $N_{Ed,max}$  on the section with respect to the variation of the alpha and beta exponents was developed. Values shown correspond to eccentricity specimens  $e=20\text{mm}$ , taken as the mean between the case studies.

For case study I, shown in Figure 32 where alpha is set equal to unity and the values of beta are varied, solutions obtained show a scatter behavior where the tendency to axial reduction still happening but this time throughout the entire curve.

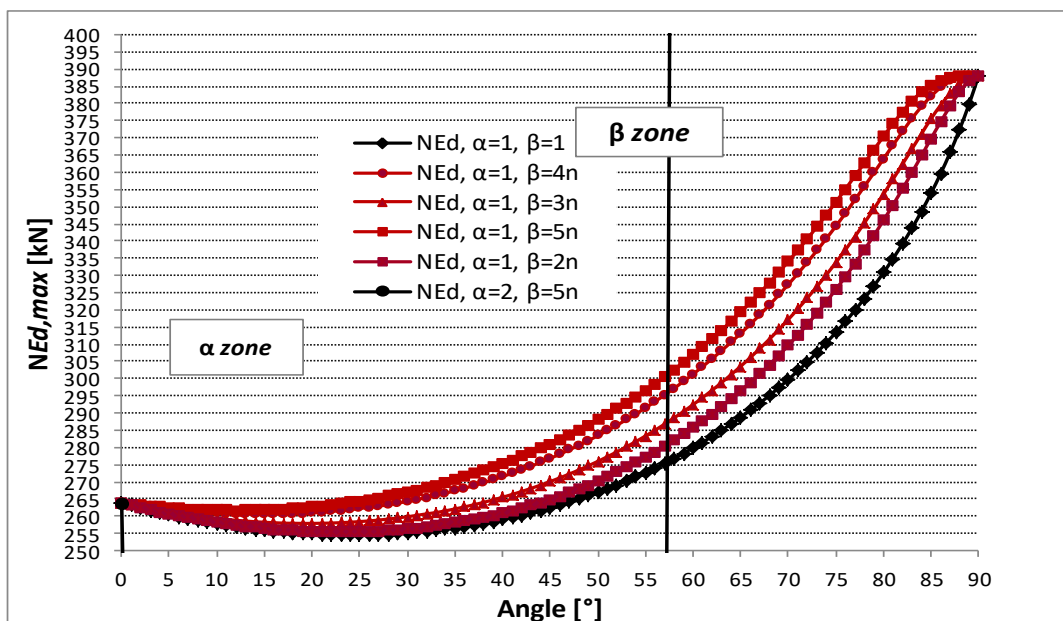


Figure 32. Sensitivity analysis case I

Case study II (Figure 33), where alpha exponent value is set equal to two and the values of beta are continued to be varied, curves show a less scatter behavior between alpha zones. Nevertheless considerable reduction of resistance ratios although less noticeable than in case I, is concentrated in the beta zone, which allows us to affirm the importance of considering  $\alpha=2$ .

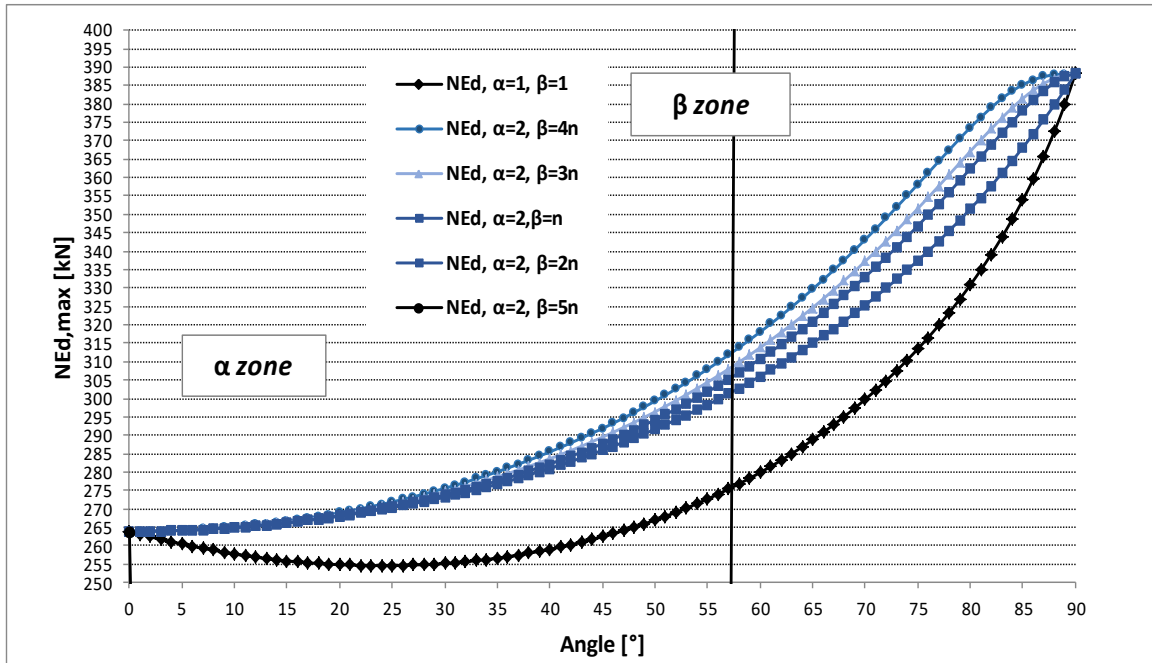


Figure 33. Sensitivity analysis case II

Finally *Figure 34* shows how results are adequate only when beta takes values equal to  $5n$ , and validates design formulae [12] given by EN-1993-1-4 (2006), stated that considering beta equal to unity is an extremely conservative criterion that should not be applied in stainless steel cross sectional studies.

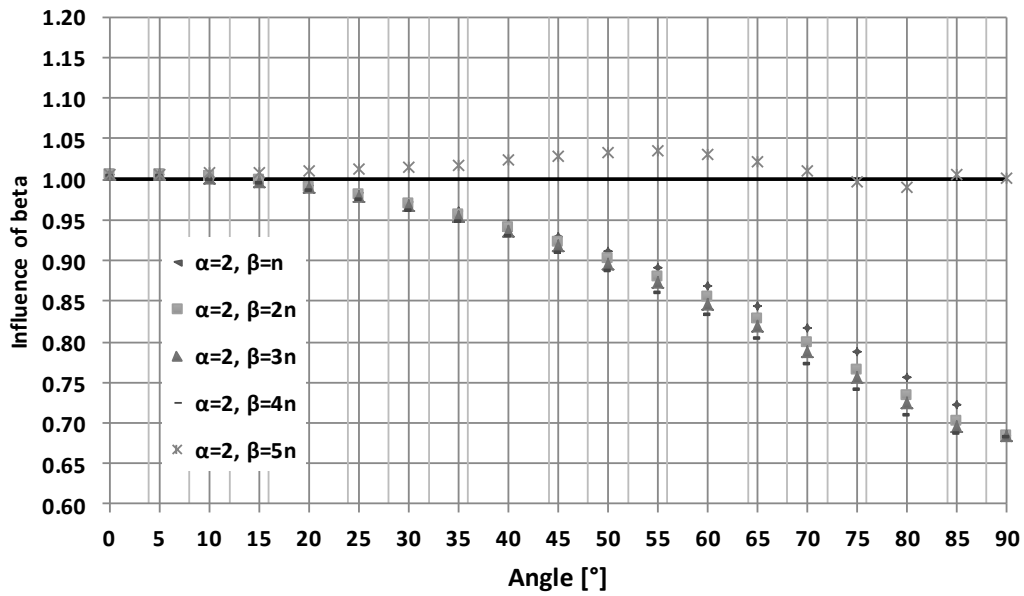


Figure 34. Influence of coefficient beta

## Chapter 6

### DISCUSSION AND CONCLUSIONS

The structural performance of austenitic stainless steel I-welded sections under biaxial compressive load has been investigated through this study with the variation of loading application points with the aim to assess design formulae proposed by European standard EN-1933-1-4.

A brief summary of stainless steel types and material response, literature review, design formulae proposed by European standards an alternative strength method and previous experimental studies in austenitic stainless steel subjected to eccentric compression load is presented in *chapter 2*. Description of experimental data, constitutive material equation and basic modelling assumptions are presented in *chapter 3*, also model validation is shown, where the use of Abaqus as a finite element program which give accuracy structural data for members eccentric loading around major axis was assessed.

Once validated structural response of members subjected to eccentric loading around major axis, model was used as a template to carry out a parametric study (*chapter 4*) related to eccentric loading around both axis to generate more beam-columns data over a wide range of load application point.

Influence of alfa and beta powers was also evaluated with a parametric study, varying the exponential values. Subsequently, phenomenological and structural analysis of the results is presented in *chapter 6*.

These have allowed assessing separately the fundamental aspects of the study: Analysis of members subjected to compression loading, analysis of members subjected to eccentric loading, influence of load application point and alfa and beta sensitivity analysis.

An appraisal of the results obtained from the perspective of the presented objectives is given herein:

### **6.1. Analysis of members subjected to compression loading.**

Analysis of numerical results allowed the accuracy of the European code EN 1993-1-4 (2006) to be assessed. It was concluded that the codified method considerably under-estimate the cross-sectional resistance of stainless steel I under compression loading, mainly owing to the consideration of  $\sigma_{0.2}$  as a proof stress.

Results of buckling reduction factors are lower than those obtained by elasticity theory. In fact EN-1993-1-4 overestimates the values of sectional resistance for non-dimensional slenderness less than 0.27. To find accuracy and consistency in predictions in results, the employment of a linear interaction curve and the adoption of conservative end points that ignore the beneficial influence of strain hardening

### **6.2. Analysis of members subjected to eccentric loading.**

With the results obtained of cross sections subjected biaxial bending whereby under radial variations between 0 and 360 degrees it is concluded that the non-linear stress-strain response increase notably in the flexural behavior of members.

Numerical models shown to yield significantly more accurate and consistent strength predictions than the codified methods.

The mean ratios of numerical to theoretical failure loads,  $N_{Ed,num}/N_{Ed,theor}$  are 1.17, 1.15 and 1.10. Increments higher than 10 percent must be consider as a large unsafety margins for engineering design.

On the other hand, Abaqus shows a quite correct physical representation of the phenomenon of study and also recognizes the parametric variation of eccentricity as a function of the angle and magnitude.



It is therefore recommended to use the subroutine developed for future studies in order to evaluate members subjected to eccentric loading.

### **6.3. Influence of load application point.**

As specimen's length increases, eccentricity magnitude influence decreases in the area close to the major axis: 45 and 90 degrees,

It is concluded that for smaller lengths, the code underestimates biaxial bending resistance of I sections between 25 and 30 percent. This confirm the conservative criteria adopted by the normative related to ultimate cross sectional capacity of I welded stainless steel profiles.

Conversely, for values of eccentricity higher than 5 mm, plastic resistance reduction produced by the axial-moment interaction increases by five percent for each magnitude of eccentricity at angles between 0 and 45 degrees, while between 45 And 90 degrees axial reduction has less scatter despite variation in the magnitude of the eccentricity.

### **6.4. Alpha and beta sensitivity analysis.**

Using the exponents related to the conservative form alpha and beta equal to unity, is not efficient from the point of view of sectional resistance due to a significant loss of  $N_{Ed,max}$  (values greater than 10 percent) is generated between 30 and 85 degrees.

It is concluded that values proposed by EN-1993-1-3 in Eq [12] related to  $\alpha=2$  and  $\beta=5\eta$ , are the ones that best fit the results obtained from the calculation program, given accurate and less scatter results for biaxial bending.

### **6.5. Future research work**

The present study has focused its attention in the cross sectional behavior of I welded austenitic stainless steel profiles subjected to biaxial loading. With the aim of expanding the study and to generate more data, it is recommended for future investigations:

- To evaluate the same model with the addition of residual stresses distribution in the numerical program, in order to investigate residual stress influence in Ultimate Load.
- To study SHS and RHS cross-sections under biaxial bending applying the same method in order to evaluate cross-sectional response and compared results.
- To perform an experimental tests in order to support the numerical results already obtained.
- To consider a wide range length, higher than 500mm to compare behavior of members.

## Chapter 7

### REFERENCES

ABAQUS FEA, Simulia© Dassault Systèmes, (2010).

AISI. (2012). AISI- S100-12. North American specification for the design of cold-formed steel structural members. American Iron and Steel Institute (AISI). Washington, D.C., 2012.

Afshan S. and Gardner L. (2013b). The continuous strength method for structural stainless steel design. *Thin-Walled Structures*, 68, 42-49.

Arrayago, I (2016). New approach for efficient design of stainless steel RHS and SHS elements. Doctoral Thesis. *Department of Civil and Environmental Engineering, Universitat Politècnica de Catalunya, Barcelona, Spain.*

Copyright © 2008 ASM International®. All rights reserved. *Stainless Steels for Design Engineers (#05231G). Austenitic Stainless Steels. Chapter 6.*

Becque J. and Rasmussen K.J.R. (2008). Numerical investigation and design methods for stainless steel columns failing by interaction of local and overall buckling. Research Report No. R888. Centre for Advanced Structural Engineering, School of Civil Engineering, The University of Sydney, Australia.

Becque J. and Rasmussen K.J.R. (2009c). Experimental investigation of the interaction of local and overall buckling of stainless steel I-columns. *Journal of Structural Engineering (ASCE)*, 135(11), 1340-1348.

Dubina D., Ungureanu V., Szabo I., 2001, Codification of imperfections for advanced finite analysis of cold-formed steel members, Proceedings of the 3rd ICTWS 2001, 179-186.

Euro Inox (2004). Pedestrian Bridges in Stainless Steel. First Edition. Building series, Vol. 7

Euro Inox (2006). Design Manual for Structural Stainless Steel. Third Edition

European Committee for Standardization. (2005). EN1993-1-1. European Committee for Standardization Eurocode 3. Design of steel structures. Part 1-1: General rules and rules for buildings. Brussels, Belgium.

European Committee for Standardization. (2006). EN1993-1-3. European Committee for Standardization Eurocode 3. Design of steel structures. Part 1-3: General rules. Supplementary rules for cold formed members and sheeting. Brussels, Belgium.

European Committee for Standardization. (2006). EN1993-1-4. European Committee for Standardization Eurocode 3. Design of steel structures. Part 1-4: General rules. Supplementary rules for stainless steels. Brussels, Belgium.

Gardner L. (2002). A New Approach to Structural Stainless Steel Design. Doctoral Thesis. Imperial College London

Gardner L. and Nethercot D.A. (2004a). Experiments on stainless steel hollow sections - Part 1: Material and cross-sectional behaviour. *Journal of Constructional Steel Research*, 60(9), 1291-1318.

Gardner L. and Ashraf M. (2006). Structural design for non-linear metallic materials. *Engineering Structures*, 28(6), 926-934.

Gardner, L. (2008a). Aesthetics, economics and design of stainless steel structures. *Advanced Steel Construction*, 4(2), 113-122.

Gardner, L. (2008b). The continuous strength method. *Proceeding of the Institution of Civil Engineers-Structures and Buildings*. 161(3), 127-133.

Liew, A. and Gardner, L. (2015). Ultimate capacity of structural steel cross-sections under compression, bending and combined loading, *Structures*, 1, 2-11.

- Liu Y. and Young B. (2003). Buckling of stainless steel square hollow section compression members. *Journal of Constructional Steel Research*, 59(2), 165-177.
- Liu Y. and Young B. (2003). Buckling of stainless steel square hollow section compression members. *Journal of Constructional Steel Research*, 59(2), 165-177.
- Lindner, J. (1984). Interaktion zwischen den vollplastischen Schnittgrößen N und My bei I-Profilen. *Stahlbau*, 53, 249-250.
- Lindner, J. (1997). Design of steel beams and beam columns. *Engineering Structures*, 19(5), 378-384.
- Lindner, J. (2003). Design of beams and beam columns. *Progress in Structural Engineering and Materials*, 5(1), 38-47.
- Mirambell E. and Real E. (2000). On the calculation of deflections in structural stainless steel beams: an experimental and numerical investigation. *Journal of Constructional Steel Research*, 54(4), 109-133.
- Rasmussen K.J.R., Burns T., Bezkorovainy P. and Bambach M.R. (2003). Numerical modelling of stainless steel plates in compression. *Journal of Constructional Steel Research*, 59, 1345-1362.
- Rubin, H. (1978). Interaktionsbeziehungen zwischen Biegemoment, Querkraft und Normalkraft für einfachsymmetrische I- und Kasten-Querschnitte bei Biegung um die starke und für doppelsymmetrische I-Querschnitte bei Biegung um die schwache Achse. *Stahlbau*, 47(3), 76-85.
- Theofanous M., Saliba N., Zhao O., and Gardner L. (2014). Ultimate response of stainless steel continuous beams. *Thin-Walled Structures*, 83, 115-127.
- Zheng B., Hua X. and Shu G. (2015). Tests of cold-formed and welded stainless steel beamcolumns. *Journal of Constructional Steel Research*, 111, 1-10.
- Zhao, O. (2015). Structural behaviour of stainless steel elements subjected to combined loading. (Thesis). *University of Hong Kong, Pokfulam, Hong Kong*.